



UNIVERSIDADE ESTADUAL DE CAMPINAS
INSTITUTO DE QUÍMICA

MARIA RODRIGUES PINTO

**BISTABILITY INDUCED BY THE PRESENCE OF 1,10-PHENANTHROLINE IN
THE ELECTRODEPOSITION OF COPPER**

**BISTABILIDADE INDUZIDA PELA PRESENÇA DA 1,10-FENANTROLINA
NA ELETRODEPOSIÇÃO DE COBRE**

CAMPINAS
2019

MARIA RODRIGUES PINTO

**BISTABILITY INDUCED BY THE PRESENCE OF 1,10-PHENANTHROLINE IN
THE ELECTRODEPOSITION OF COPPER**

**BISTABILIDADE INDUZIDA PELA PRESENÇA DA 1,10-FENANTROLINA
NA ELETRODEPOSIÇÃO DE COBRE**

Dissertação de Mestrado apresentada ao Instituto de Química da Universidade Estadual de Campinas como parte dos requisitos exigidos para a obtenção do título de Mestra em Química na área de Físico-Química

Master's Dissertation presented to the Institute of Chemistry of the University of Campinas as part of the requirements to obtain the title of Master in Chemistry in the area of Physical-Chemistry.

Supervisor: Prof. Dr. Raphael Nagao de Sousa

O arquivo digital corresponde à versão final da Dissertação defendida pela aluna Maria Rodrigues Pinto e orientada pelo Prof. Dr. Raphael Nagao de Sousa.

**CAMPINAS
2019**

Ficha catalográfica
Universidade Estadual de Campinas
Biblioteca do Instituto de Química
Camila Barleta Fullin - CRB 8462

P658b Pinto, Maria Rodrigues, 1995-
Bistability induced by the presence of 1,10-phenanthroline in the
electrodeposition of copper / Maria Rodrigues Pinto. – Campinas, SP : [s.n.],
2019.

Orientador: Raphael Nagao de Sousa.
Dissertação (mestrado) – Universidade Estadual de Campinas, Instituto de
Química.

1. Eletroquímica. 2. Eletrodeposição. I. Sousa, Raphael Nagao de. II.
Universidade Estadual de Campinas. Instituto de Química. III. Título.

Informações para Biblioteca Digital

Título em outro idioma: Bistabilidade induzida pela presença da 1,10-fenantrolina na
eletrodeposição de cobre

Palavras-chave em inglês:

Electrochemistry

Electrodeposition

Área de concentração: Físico-Química

Titulação: Mestra em Química na área de Físico-Química

Banca examinadora:

Raphael Nagao de Sousa [Orientador]

Juliano Alves Bonacin

Ernesto Chaves Pereira de Souza

Data de defesa: 11-07-2019

Programa de Pós-Graduação: Química

Identificação e informações acadêmicas do(a) aluno(a)

- ORCID do autor: <https://orcid.org/0000-0003-3453-795>

- Currículo Lattes do autor: <http://lattes.cnpq.br/2033028451837954>

BANCA EXAMINADORA

Prof. Dr. Raphael Nagao de Sousa (Orientador)

Prof. Dr. Juliano Alves Bonacin (Instituto de Química - UNICAMP)

Prof. Dr. Ernesto Chaves Pereira de Souza (Departamento de Química - UFSCar)

A Ata da defesa assinada pelos membros da Comissão Examinadora, consta no SIGA/Sistema de Fluxo de Dissertação/Tese e na Secretaria do Programa da Unidade.

Este exemplar corresponde à redação final da Dissertação de Mestrado defendida pela aluna Maria Rodrigues Pinto, aprovada pela Comissão Julgadora em 11 de julho de 2019.

DEDICATORY

“I dedicate this work to my parents, José Geraldo and Nilza and my brother Pedro. Thank you for all your support and trust during all these years.”

ACKNOWLEDGEMENTS

This dissertation is the result of all the learning acquired during my entire education and the contribution of all the people who crossed my path, people who I met in Campinas during all those years and also to all to everyone I brought in my heart from Coronel Fabriciano and all the Vale do Aço. First, I would like to thank my parents, José Geraldo and Nilza Rodrigues and also my brother Pedro for being my main motivators and for supporting me on this journey. Special thanks to professor Dr. Raphael Nagao for his guidance, for placing his trust in me and my work, for investing in my professional training in every way.

Thanks to CampEG, the electrochemistry group of the Institute of Chemistry, I am very proud to be present practically from the beginning of the group and see how much we have achieved in such a short time. To all who are and have passed through the group: prof. Dr. Pablo, Aline, Adriana, Caio Guilherme, Carlos, Celso, Cléo, Eduardo Machado, Hamsa, Gustavo, Igor, José Luís, Laura, Matheus, Marta, Raquel, Renan, Wesley, Bianca, Caio Rodrigues, Eduardo Parma, Guilherme, Jaqueline, Rafael, Victor and others that I may have failed to mention. Special thanks to Júlia, who was my partner during this work, it was a pleasure to teach and learn from you. Thanks to all my friends from college, especially Guilherme, Isabela Sato, Isabela Sanches and Fernanda; my friends of the LCN futsal and basketball team, partners on the court and in life; the girls from apartment 51, former and current, Isadora, Ingrid, Ludmila e Bianca; my aunts Luíza and Cláudia and my cousins Isabela, Maria Luíza and Matheus. I could not fail to mention CEFET-MG, where my journey through chemistry began. I am very grateful for the opportunity to study at a high-level federal school with master and doctor teachers who taught us to dream high. During those three intense years I am proud to say that I made such good friends that I will take for a lifetime. To all the people I met during the disciplines, courses, conferences, congresses, seminars, or meetings, where enriching and primordial discussions about science were held and friendships were made.

I thank the Institute of Chemistry and the entire University of Campinas, for the environment of excellence and for all the institutions responsible for building and maintaining such an important center for Brazilian research.

This study was financed in part by the Coordenação de Aperfeiçoamento de Pessoal de Nível Superior - Brasil (CAPES) - Finance Code 001.

Thanks to the São Paulo Research Foundation (FAPESP, process: 2017/05592-4) for the scholarship granted.

EPIGRAPH

“We must not forget that when radium was discovered no one knew that it would prove useful in hospitals. The work was one of pure science. And this is a proof that scientific work must not be considered from the point of view of the direct usefulness of it. It must be done for itself, for the beauty of science, and then there is always the chance that a scientific discovery may become like the radium a benefit for humanity.”

Marie Curie

RESUMO

É estudado em detalhe o efeito inibitório na reação de eletrodeposição de cobre causado pela adsorção da 1,10-fenantrolina (phen), uma molécula N-heterocíclica, sobre a superfície de cobre metálico devido a fortes interações entre os átomos de nitrogênio da molécula e o substrato. Mesmo pequenas adições de phen no meio reacional alteram significativamente a velocidade da reação faradaica. Observamos que a inibição induzida pela phen durante a eletrodeposição de cobre acarretou uma instabilidade dinâmica conhecida como bistabilidade em uma ampla gama de parâmetros estudados. A instabilidade foi classificada e validada pela análise de Espectroscopia de Impedância Eletroquímica. Sob a perspectiva molecular, a massa molar aparente dos adsorventes no domínio da bistabilidade foi calculada através do monitoramento gravimétrico realizado na Nanobalança Eletroquímica de Cristal de Quartzo, os resultados indicam que as mudanças de massa ocorrem principalmente devido à redução dos íons cobre bivalentes dissolvidos no meio reacional. É importante ressaltar que a adsorção de moléculas phen protonadas não possui uma contribuição significativa em variações de massa, mas impede a formação de uma morfologia de grãos de cobre sobre a superfície. Imagens de Microscopia Eletrônica de Varredura indicam nódulos mais finos no ramo inferior em comparação com o ramo superior no domínio da bistabilidade. Com base nessas observações, um mecanismo cinético é proposto, e uma boa concordância é obtida entre a massa molar aparente extraída de experimentos e os valores teóricos. Em conjunto, nossos resultados contribuem para uma descrição físico-química detalhada do comportamento não-linear, trazendo novas contribuições sobre essa reação e trazendo a possibilidade de projetar eletrodos com superfície mutáveis utilizando-se do comportamento biestável para tal.

ABSTRACT

The inhibiting effect in the electrodeposition of copper resulted from the adsorption of 1,10-phenanthroline (phen), an N-heterocyclic organic molecule, on metallic copper surface due to strong interactions between the nitrogen atoms and the substrate is studied in detail. Even small additions of phen in the reaction media alters significantly the faradaic rate. We have found that the inhibition induced by phen during the electrodeposition of copper originated a dynamic instability known as bistability in a wide range of studied parameters. The instability was classified and validated by Electrochemical Impedance Spectroscopy analysis. Under the molecular perspective, the apparent molar mass of the adsorbents in the bistability domain was calculated using Electrochemical Quartz Crystal Nanobalance monitoring in the electrochemical experiments and the results indicate that mass changes occur mainly due to the reduction of copper from bivalent ions dissolved in the reaction media. Importantly, the adsorption of protonated phen molecules does not show a considerable contribution in mass variations but prevents the formation of a copper coarse grained morphology over the surface. Scanning Electron Microscope images indicates finer nodulations at the lower branch compared to the upper branch in the bistability domain. On the basis of these observations, a kinetic mechanism is proposed, and a good agreement is obtained between the apparent molar mass extracted from experiments and the theoretical values. Altogether, our results contribute to a detailed physical chemical description of the nonlinear behavior, bringing new insights about this reaction and pointing out the possibility to design switchable surface electrodes by taking advantage of the bistable behavior.

LIST OF ILLUSTRATIONS

Figure 1: Simplified equivalent circuit for an electrochemical cell. Adapted from Krischer, K. Varela, H. Oscillations and other dynamics instabilities. In: Handbook of fuel cells: fundamentals, technology and applications, v.2. Ed. Chichester. John Wiley & Son ²⁷	23
Figure 2: Location of the saddle-node bifurcation separating monostable and bistable regions in the E/R_{ext} parameter plane. (SN = saddle-node bifurcation, c = cusp point). Adapted from Krischer, K., Nonlinear Dynamics in Electrochemical Systems. In: Advances in Electrochemical Science and Engineering, Volume 8. Edited by Alkire, R. C. ³³	25
Figure 3: Structural representation of 1,10-phenanthroline.	27
Figure 4: Scheme of a three-array electrochemical cell with the Work Electrode (WE), Counter Electrode (CE) and Reference Electrode (RE).	32
Figure 5: Scheme of a cyclic voltammetry showing the Start Potential, the Upper Potential and the Lower Potential. The slope corresponds to the scan rate, dE/dt of the cyclic voltammetry.	33
Figure 6: (a) Cyclic voltammograms of the Pt H ₂ SO ₄ system at $dE/dt = 0.05 \text{ V s}^{-1}$ in the potential window: (a) 0.05 to 1.30 V. (b) Same as item (a) but with scan rate of 0.01 V s^{-1} and with the addition CuSO ₄ . [H ₂ SO ₄] = 0.5 mol L ⁻¹ and [CuSO ₄] = 0.5 mol L ⁻¹ . The arrows indicate the sweep direction.	37
Figure 7: Cyclic voltammograms of the Pt H ₂ SO ₄ ,CuSO ₄ system at $dE/dt = 0.01 \text{ V s}^{-1}$ in the potential window: -0.10 to 0.30 V (black line); but with addition of 2.0 mmol L ⁻¹ of phen (red line). [H ₂ SO ₄] = 0.5 mol L ⁻¹ and [CuSO ₄] = 0.5 mol L ⁻¹ . The arrows indicate the sweep direction.	38
Figure 8: Cyclic voltammetry of the Pt H ₂ SO ₄ ,CuSO ₄ ,phen system at $dE/dt = 0.01 \text{ V s}^{-1}$ in the potential window: (a) -0.10 to 0.20 V, (b) -0.10 to 0.30 V, (c) -0.10 to 0.40 V, (d) 0 to 0.30 V, (e) -0.20 to 0.30 V, (f) -0.30 to 0.30 V. [H ₂ SO ₄] = 0.5 mol L ⁻¹ , [CuSO ₄] = 0.5 mol L ⁻¹ and [phen] = 2.0 mmol L ⁻¹	40
Figure 9: Cyclic voltammograms at $dE/dt = 0.01 \text{ V s}^{-1}$ under different external resistances at phen = 2.0 mmol L ⁻¹ and $R_{ext} =$ (a) 7, (b) 14, (c) 21, (d) 28 $\Omega \text{ cm}^2$ and under the effect of the	

concentration of phen at $R_{ext} = 28 \Omega \text{ cm}^2$ and phen = (e) 0.5, (f) 1.0, (g) 1.5 and (h) 2.0 mmol L^{-1} . The arrows indicate the direction of the sweep..... 42

Figure 10: Bifurcation diagram R_{ext} vs E measured with $dE/dt = 0.01 \text{ V s}^{-1}$ in several concentrations of phen: 0.5 (green line), 1.0 (blue line), 2.0 mmol L^{-1} (red line)..... 43

Figure 11: Bifurcation diagram R_{ext} vs. E measured at sweep rate of $dE/dt = 0.01 \text{ V s}^{-1}$ in two concentrations of phen: 1.5 mmol L^{-1} (purple dots) and 2.0 mmol L^{-1} (red dots)..... 44

Figure 12: Nyquist plots for the electroreduction of Cu without (black lines) and with (red lines) phen molecules in the concentration of 2.0 mmol L^{-1} at the applied voltages: (a) 0.24, (b) 0.12 and (c) -0.05 V. The insets correspond to a “zoom in” on the plates a-c. 46

Figure 13: Current densities (dashed line) and mass variations (full line) at $dE/dt = 0.02 \text{ V s}^{-1}$ with additions of phen as final concentration of (a) 0 (black), (b) 0.5 (green), (c) 1.0 (blue), (d) 2.0 mmol L^{-1} (red). $[\text{H}_2\text{SO}_4] = 0.5 \text{ mol L}^{-1}$ and $[\text{CuSO}_4] = 0.5 \text{ mol L}^{-1}$. The arrows indicate the direction of the sweep..... 48

Figure 14: (a-d) j vs E and (e-h) Δm vs q in the potential interval of 0 to 0.20 V. The arrows indicate the direction of the sweep. The curves follow the color code used in the text for phen concentrations: 0 (black), 0.5 (green), 1.0 (blue) and 2.0 mmol L^{-1} (red). The gray bands represent the potential window where mass/charge ratios were calculated. 50

Figure 15: (a) j vs E , (b) Δm vs E , (c) Δm vs q in the potential interval of 0-0.20 V in the absence of CuSO_4 . The curves follow the color code used as previously: 0.5 (green), 1.0 (blue) and 2.0 mmol L^{-1} (red). $[\text{H}_2\text{SO}_4] = 0.5 \text{ mol L}^{-1}$ 52

Figure 16: Cyclic voltammetry of the $\text{Cu}|\text{H}_2\text{SO}_4$ (black line) and $\text{Cu}|\text{H}_2\text{SO}_4,\text{phen}$ (blue line) systems at $dE/dt = 0.02 \text{ V s}^{-1}$ in the potential window of 0 to 0.20 V. $[\text{H}_2\text{SO}_4] = 0.5 \text{ mol L}^{-1}$ and $[\text{phen}] = 1.5 \text{ mmol L}^{-1}$ 53

Figure 17: Electronic micrographs of the electrode surface after the electrodeposition of Cu perturbed with 2.0 mmol L^{-1} of phen. The samples were obtained at the potentials of 0.24 (SSI), 0.12 (BS_u and BS_d as the upper and lower branches of the BS domain, respectively) and -0.05 V (SSII). The diameter of all images is 9 μm 54

LIST OF ABBREVIATIONS AND ACRONYMS

bp	Bifurcation Point
BS	Bistability
CE	Counter Electrode
ECSA	Electrochemically Active Surface Area
EIS	Electrochemical Impedance Spectroscopy
EQCN	Electrochemical Quartz Crystal Nanobalance
HB	Hopf Bifurcation
HN-NDR	Hidden N-Shaped Negative Differential Resistance
NDR	Negative Differential Resistance
N-NDR	N-Shaped Negative Differential Resistance
phen	1,10-Phenanthroline
Pt-H	Hydrogen Adsorbed at Platinum Surface
Pt-O	Oxygen Adsorbed at Platinum Surface
Q_{ox}^H	Charge due to the Oxidation of Adsorbed Hydrogen
RE	Reference Electrode
RHE	Reversible Hydrogen Electrode
SEM	Scanning Electron Microscopy
SN	Saddle-Node
S-NDR	S-Shaped Negative Differential Resistance
SSI	Steady State I
SSII	Steady State II
WE	Working Electrode

LIST OF SYMBOLS

Δf	Resonating Frequency Variation
Δm	Mass Variation
ΔQ	Charge Density
Δt	Time interval
μ_c	Shear Modulus
C	Surface Concentration of Electroactive Species
C_{DL}	Double Layer Capacitance
E	Supplied potential by the Potentiostat
F	Faraday Constant
f_o	Fundamental Quartz Crystal Frequency
I	Current
I_C	Capacitive Current
I_F	Faradaic Current
$Im(Z)$	Imaginary Component of Impedance
j	Current density
j_o	Exchange Current Density
k	Constant Rate of the Reaction
m/z	Mass/Charge Ratio
M_{app}	Apparent Molar Mass
MM	Molar Mass
n	Number of Electrons Transferred
R	Equivalent Resistance
R_{crit}	Critical Resistance
R_{ext}	External Resistance
R_{Ω}	Ohmic drop resistance
$Re(Z)$	Real Component of Impedance
t	Time
T	Absolute Temperature
v_v	Scan Rate

z	Ion Electrovalence
Z	Impedance
Z_F	Faradaic Impedance
α_a	Anodic Charge Transfer Coefficient
α_c	Catodic Charge Transfer Coefficient
$\delta\phi$	Potential Perturbation from Steady State
κ	Calibration Constant of EQCN
ρ_c	Quartz Density
ϕ	Potential at the Surface of the Work Electrode
ϕ_{eq}	Equilibrium Potential of the Electrochemical Reaction
ϕ_{ss}	Steady State Surface potential
ω	Frequency of Perturbation

CONTENTS

1. Introduction	16
1.1. Importance of self-organization in materials science	16
1.2. Dynamical instabilities in electrochemical systems	18
1.2.1. Emergence of bistability	22
1.3. Effect of organic molecules in electrodeposition systems	27
2. Objectives.....	30
3. Methodology	31
3.1. Electrochemical system	31
3.1.1. Cyclic voltammetries	32
3.1.2. Electrochemical Impedance Spectroscopy	33
3.1.3. Electrochemical Quartz Crystal Nanobalance	33
3.2. Imaging Analysis	35
4. Results and discussion.....	36
4.1. Cyclic voltammetries and bifurcation diagrams	36
4.2. Electrochemical Impedance Spectroscopy characterization.....	44
4.3. Gravimetric analysis	47
4.4. Scanning Electron Microscopy analysis	53
4.5. Mechanistic Interpretation	55
5. Conclusion.....	59
5.1. General conclusions	59
5.2. Perspectives	60
6. Bibliography.....	61
7. Supplementary information.....	72

1. Introduction

1.1. Importance of self-organization in materials science

A wide range of materials can be synthesized by electrodeposition techniques, in which an electric current is used to reduce dissolved cations in a homogeneous solution over a conductive material as the substrate.¹ Systems in which the dynamic cannot be simply described by linear differential equations, contain what we call dynamical instabilities, these sort of system can be an important resource to obtain nanostructured materials with unique compositions,²⁻⁴ such as: multilayered materials of different metals, alternated multilayers of Cu and Sn,⁴ alternated multilayer between metal oxides and metal, as Cu and Cu₂O⁵⁻⁸ or patterned alloy of Ag and Sb.⁹ Combining materials that possesses different properties can be useful to form, for instance, an electronic device that can be suitable for its conductivity through quantum tunneling.⁸ It has been reported before the use of alternated multilayer of Cu and Cu₂O for glucose detection¹⁰ and also in Li-ion batteries¹¹. The possibility of easy control of the experimental parameters makes the electrochemical system attractive for the synthesis of these nanostructured materials.

As stated by Orlik¹² a system that presents spontaneous formation of order in the time and/or space domain when kept far from the equilibrium can be labeled as a dynamic self-organization system. This condition can be ascribed in two main reasons, the first one is the thermodynamic, described by Prigogine.¹³ The decrease in the entropy due to the gain of order in a system must be at least compensated in some way, which is described as a dissipative structure. The second one is the kinetic component, that must meet the conditions of having a nonlinear dependence between driving forces and resulting flows and the existence of an autocatalytic and/or autoinhibition component.¹²

One of the most famous example of an oscillating reaction that generates spatial and temporal patterns is the Belousov-Zhabotinsky reaction.^{12,14} In fact the modern nonlinear chemical dynamics studies can be traced out to Belousov, that first observed the oscillation reaction in 1950.¹⁵ He carefully studied the system and its dependence with the temperature and reactants initial concentrations and observed travelling waves with contrasting colors. For several years that were many studies concerning the detailed aspects of the BZ reaction, but no mechanism, where the first mechanism attempt was only first reported in 1972 by Field and Noyes.¹⁶ In the course of the reaction, there is a spontaneous emergency of waves, representing

the diffusion of the species in the medium. During the experiment the waves are clearly observed, but once the reaction reaches the equilibrium the patterns fade away, so it is only possible to analyze the patterns through *in-situ* techniques.²

This work is focused in the nonlinear dynamics in a specific electrodeposition system. Electrodeposition systems are convenient because the patterns that can be formed during the reaction remain on the surface of the substrates even after the reaction is interrupted. In that fashion, it is possible to analyze the patterns formed through others *ex-situ* techniques, such as scanning or transmission electronic microscope.^{2,9,17,18} The study of the dynamics and the instabilities behind electrodeposition processes allow the design of materials orientated to their application, whence their attributes that can benefit in some sense the process can be improved.¹⁰

Complex systems are inherently sensitive to the experimental parameters and small changes can affect drastically the observed dynamics and even the physical properties of the material.¹⁹ Consequently, chemical switches can be designed and finely tuned by the imposition of external perturbations.²⁰⁻²⁴ It is important to understand how the system is affected by the different experimental variables – such as nature of electroactive species, temperature, current and potential – to elaborate an hypothesis about the step-by-step mechanism behind the observed phenomena which are not always clear in all systems. The studies in the respect of electrochemical nonlinear systems are still very recent, and in fact, systems concerning new types of oscillations and bistabilities are daily reported.^{25,26} The most common approach in these studies is based on univariate changes in one specific parameter while others are kept constant, but this method, however, may hide synergic combinations among the parameters, since the correlation between parameters and response is not always linear. The development of biomimetic or smart materials require an accurate control of the oscillation frequency and that is why is so important to acquire a deep understanding of the electrochemical mechanism of the systems. A very modern challenge in material science is to correlate the physicals properties of an given material, such as thickness and composition, to its thermodynamic behavior.⁷

1.2. Dynamical instabilities in electrochemical systems

There are many electrochemical systems that present nonlinear dynamical behavior when they are far from the condition of thermodynamic equilibrium.²⁷ In heterogeneous systems, processes placed in the electrode/solution interface can undergo through dynamical instabilities under certain experimental conditions.¹² All phenomena of this type are deeply correlated with the stability of the states, in that matter, it is important to distinguish between the terms steady state and stable state. The first one, also named as fixed point, means that the characteristics of that state do not change as a function of time. The stable state can be of two different types, a steady stable state, also known as a stable fixed point or an attractor, where the steady state is resistant to external perturbations, that undergo through damping, until the system returns to its original state.²⁷ The steady state can also be unstable, also called unstable fixed point or repeller, that do not survive to fluctuations in the system, when they experience any type of perturbation, they moved forward to the nearest attractor point. A stable state is necessarily correlated to the thermodynamic equilibrium, it is a particular example of a steady state.¹²

The dynamical instabilities observed in electrochemical systems are correlated to the so-called negative differential resistance (NDR)²⁸ – the I (current) vs φ (electrode potential) curve presents a region containing a negative slope. It is essential to point out at this moment the difference between the electrode potential and the external voltage applied by the potentiostat, here denoted as E . Where φ stands for the potential drop at the working electrode/solution interface, the dependence between these two parameters is expressed in the equation of the load line (Eq. 1):¹²

$$E = \varphi + IR \quad \text{Eq. 1}$$

In which the resistances exhibited in the electrochemical systems are summarized to a single value of an equivalent resistance, R , connected in series with the cell. The equivalent circuit of an electrochemical cell will be explained in detail in the next subsection.

The phenomenon of bistability (BS), defined by two stable steady states that exist at the same set of controlling parameters is observed in the presence of a NDR. If more than two steady states are present in a certain range of control parameters this phenomenon is called multistability.¹² The NDR arises mainly due to the electrical autocatalysis in the electrode

potential as the essential positive feedback variable.²⁹ The addition of a negative feedback loop to the system may lead to simple periodic oscillations²⁷ and chaos can be observed as well when multiples – more than two – are acting in the system.¹⁴ According to Koper³⁰ there are more than one possible cause to the appearance of the NDR, which can be verified from the faradaic current of a process (I_F):

$$I_F = nFA(\varphi)k(\varphi)C(\varphi) \quad \text{Eq. 2}$$

In Eq. 2 n stands for the number of the electrons transferred in the reaction, F is the Faraday constant, A is the available electrode area, k is the rate constant of the reaction and C is the surface concentration of the electroactive species, where the last three are dependent from electrode surface potential (φ). In the region where the NDR is present, at a I/φ curve, when φ is increased, a decrease in I_F is observed, so in order to meet that condition:

$$\frac{dI_F(\varphi)}{d\varphi} < 0 \quad \text{Eq. 3}$$

Since we have three potential dependent variables:

$$\frac{dA(\varphi)}{d\varphi} < 0 ; \quad \frac{dk(\varphi)}{d\varphi} < 0 ; \quad \frac{dC(\varphi)}{d\varphi} < 0 \quad \text{Eq. 4}$$

According to the inequalities in Eq. 4, there are three possible causes for the existence of a NDR:

- **Condition I:** first inequality, a negative slope in the $dA/d\varphi$ curve. The available electrode area decreases when the electrode polarization is increased. One very prominent example is the oxide layer formation in the electrodisolution of metals,³⁰ the oxide passivates the surface, restraining the anodic reaction. The adsorption of an poisoning species, for instance a surfactant, in the electrode surface is also a possible cause for this event.³¹
- **Condition II:** a negative slope in the $dk/d\varphi$ curve, second inequality. An increase of the double layer potential promotes a decrease in the electrochemical rate constant. There are two main examples for meeting

these conditions, the first one is the potential-dependent desorption of catalyst²⁷ and the second one is the adsorption of a non-ideal inhibitor that can cause a certain decrease in the rate constant, but does not completely hinders the reaction.¹² The dependence between the current and the electrode potential in an electrochemical reaction is expected and described by the Butler-Volmer equation (Eq. 5), known as the central equation of phenomenological electrode kinetics:³²

$$j = j_o \left[e^{-\frac{\alpha_a n F}{RT}(\varphi - \varphi_{eq})} - e^{-\frac{\alpha_c n F}{RT}(\varphi - \varphi_{eq})} \right] \quad \text{Eq. 5}$$

Where in this equation j is the current density, j_o stands for the exchange current density, α_a and α_c are the so-called anodic and cathodic charge transfer coefficient, respectively, as before n is the number of electrons involved in the electrode reaction, F is the Faraday constant, R is universal gas constant, T is the absolute temperature, φ_{eq} is the equilibrium potential of the electrochemical reaction.

- **Condition III:** third inequality, negative $dC/d\varphi$; This condition is observed in low ionic strength where the interfacial concentration of the electroactive species decreases when the electrode polarization is increased, as pointed out by Frumkin.^{2,12} This effect is due to the electric potential difference between the reaction site, in the interface, and the electric potential in the bulk solution. Cations undergoing through oxidation in a positively charged surface and anions going through reduction in negatively charged surfaces may lead to negative slope in the $dC/d\varphi$ curve in certain ranges of potential.¹²

There is more than one possible manner for the manifestation of the NDR phenomenon in an electrochemical system. In fact the negative slope in the I/φ curve might be in a N-shape or S-shape, named as N-NDR and S-NDR, respectively, where the curvatures of the diagram resembles the shape of the respective letter.¹² The different aspects of the current/electrode potential curve are related to the electrochemical aspects of the system, where in the N-NDR the electrode potential, φ is an autocatalytic variable and an inhibitory one in the

S-NDR systems. The main characteristics of these two types of NDR are described by Krischer³³, the three major characteristics of the N-NDR are:

- a) Under-potentiostatic control a N-shaped current/potential curve is obtained for vanishing values of ohmic resistance.
- b) The second characteristic is that oscillations can be seen around the branch of negative slope for intermediate values of resistance.
- c) Bistable behavior can be observed in two different conditions, under potentiostatic control with very large values of ohmic resistance and also under galvanostatic control.

The S-NDR systems are considered complementary to the N-NDR in most dynamic aspects, their essential properties are:

- a) For vanishing ohmic series resistance the systems present a stationary S-shaped I/φ curve, that is, the system contains a bistable region for some values of φ . This branch cannot be detected in experiments under potentiostatic control.
- b) If the ohmic series resistance, R_{Ω} , exceeds a critical value, the I/φ curve become single-valued, where oscillations may or not be observed around the steady states with intermediate current values.
- c) A S-NDR system can oscillate under galvanostatic control, when the current value is inside the NDR branch domain. The NDR branch is not accessible experimentally, under galvanostatic control only a hysteresis in the stationary I/φ curve is observed.

There is also a particular case of the N-NDR system, which is called the HN-NDR, the letter H stands for the word Hidden.³³ The HN-NDR system can be interpreted as being a subsystem with a N-shaped stationary polarization curve, in which the NDR is partly or entirely hidden by a slow step, which is potential dependent.¹² The slow step is often credited to the adsorption of a species that inhibits the main faradaic reaction.²⁷ Once again, we can summarize the major properties of the system in three topics:³³

a) For very small values of ohmic series resistance the I/φ stationary curve possesses a positive slope, where all states on this branch are stable, that is, oscillations do not occur in that condition. At the zero frequency perturbation, $\omega = 0$, the impedance, Z , is strictly positive, that is, $Z(\omega = 0) > 0$.

b) Current oscillations occur around the positive branch when the ohmic series resistance, R_Ω , exceeds a critical value. The oscillations are attributed to a negative real faradaic impedance, for finite frequency perturbations values, $Re(Z(\omega \neq 0)) < 0$.

c) The major difference between the N-NDR and HN-NDR systems is that oscillations can occur in both potentiostatic and galvanostatic control in the last one.

1.2.1. Emergence of bistability

The simplest dynamical instability observed in nonlinear systems is the BS phenomenon, that occurs when positive feedback loops act as regulatory steps in the overall electrochemical mechanism.³⁴ For spatially extended systems, the appearance of collective switching between states has been based on the bistable nature of the individuals,^{35–38} but it can also emerge from the collective behavior even if the constituents are not bistable.³⁹ This co-existence of different steady states has been verified in homogeneous^{40–44} and heterogeneous systems.^{45–47} BS can be encountered in both potentiostatic and galvanostatic regimes in N-NDR systems,³³ but we are going to focus only on the potentiostatic control, that will be used forward in our experiments.

To discuss the conditions required for the emergency of the BS, **Figure 1** presents a scheme of an equivalent electric circuit of an electrochemical cell.

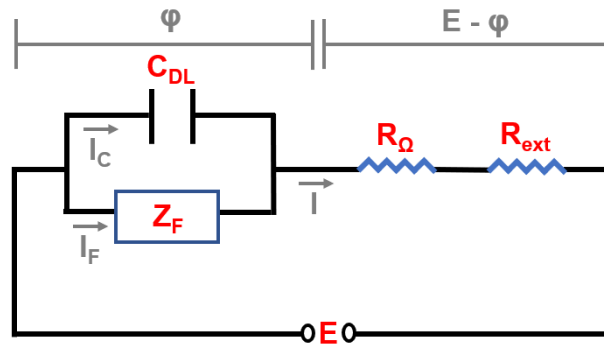


Figure 1: Simplified equivalent circuit for an electrochemical cell. Adapted from Krischer, K. Varela, H. Oscillations and other dynamics instabilities. In: Handbook of fuel cells: fundamentals, technology and applications, v.2. Ed. Chichester. John Wiley & Son²⁷

Where C_{DL} is the double layer capacitance, Z_F is the faradaic impedance, R_{Ω} resistance attributed to ohmic drop, R_{ext} is the external resistance that can be added to the system, E is the potential applied by the potentiostat, ϕ is electrode surface potential, I , I_C and I_F are the total current, capacitive and faradaic component of current, respectively.

The supplied voltage applied by the potentiostat is composed of the potential across the double layer and the uncompensated and external resistances, respectively R_{Ω} and R_{ext} , as seen before in the Eq. 1, where $R = R_{\Omega} + R_{ext}$.

Applying Kirchhoff's law in the circuit represented in **Figure 1** we obtain Eq. 6 for the total current that is equal to the sum of the capacitive and faradaic currents:

$$I = I_C + I_F(\phi) \quad \text{Eq. 6}$$

Using Eq. 6 in Eq. 1, the equation of the load line, and knowing that $I_C = C_{DL} \frac{d\phi}{dt}$ we obtain:

$$\frac{E - \phi}{R} = C_{DL} \frac{d\phi}{dt} + I_F(\phi) \quad \text{Eq. 7}$$

A steady state is achieved when $\frac{d\phi}{dt} = 0$, that condition is met when, from a ϕ vs I curve, whenever a N-shaped curve is observed. At this condition the curve has at least three

steady states or fixed points (the maximum, minimum and inflexion point). The stability analysis can be obtained from a small perturbation ($\delta\varphi$) from the stationary state (φ_{ss}), from that, in this condition, we get Eq. 8:

$$\varphi = \varphi_{ss} + \delta\varphi \quad \text{Eq. 8}$$

If $\delta\varphi$ is sufficiently small, the corresponding faradaic current can be evaluated from an expansion using a Taylor series, and respond linearly as:

$$I_F(\varphi) = I_F(\varphi_{ss} + \delta\varphi) = I_F(\varphi_{ss}) + \delta\varphi \times \left. \frac{dI_F(\varphi)}{d\varphi} \right|_{\varphi=\varphi_{ss}} \quad \text{Eq. 9}$$

In the stationary state $d\varphi_{ss}/dt = 0$, so rearranging Eq. 7 yields:

$$C \frac{d\delta\varphi}{dt} = \frac{E - (\varphi_{ss} + \delta\varphi)}{R} - I_F(\varphi) \quad \text{Eq. 10}$$

By definition $\frac{dI_F(\varphi)}{d\varphi} = Z_F^{-1}$,²⁷ substituting Eq. 9 into Eq. 10 and taking the definition into account:

$$C \frac{d\delta\varphi}{dt} = -(Z_F^{-1} + R^{-1}) \delta\varphi \quad \text{Eq. 11}$$

If $Z_F^{-1} + R^{-1} < 0$, the perturbation ($\delta\varphi$) will grow and then the steady state is classified as unstable, for that both $Z_F^{-1} < 0$ and $R^{-1} > |Z_F|$ must be fulfilled simultaneously. From the first inequality we conclude that an unstable state must lie in the negative slope region of an NDR. The second inequality means that the unstable point can only be reached if the resistance of the system is larger than the faradaic impedance of the reaction, Z_F .

Even a small perturbation from the middle unstable fixed point will drive the system to one of the others stationary states, which are stable (they belong in a region with a positive slope). The BS is manifested in a hysteresis in the I vs E plot, where, in the same set of φ , it is possible to obtain two different corresponding values of current. In the BS region, the steady state that the system will achieve, depends not only of the studied parameter (*e.g.* potential) but also the “history” of the changes,¹⁴ in this case on the potential sweep direction.

The two stable steady states form the borders of the Saddle-Node (SN) bifurcation.²⁷ The bifurcation phenomenon can be defined as the change that occur in a system when it changes from one stationary state to a bi or multi stable states, or an oscillatory state.¹⁴ A mapping of this bifurcation region can be observed in a so-called bifurcation diagram, represented in **Figure 2**. The SN bifurcation is characterized by the manifestation of two stationary states, represent by the red lines in **Figure 2**, that meet in a point called cusp point, the blue dot symbolized as c in the **Figure 2**, and that spread out as we increase a controlling parameter (for instance R_{ext}) and disappear as we decrease it.²⁷ In SN bifurcations, the system moves from one outer branch to the other; the middle branch is not accessible experimentally.

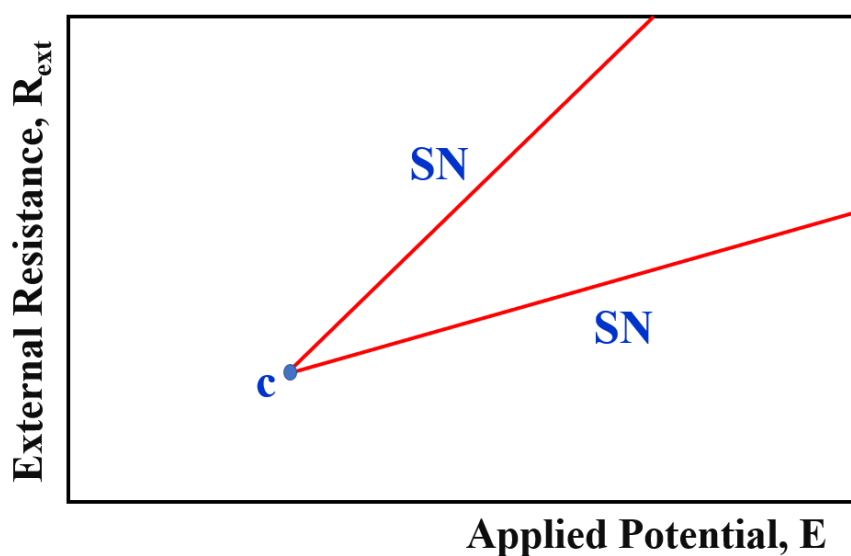


Figure 2: Location of the saddle-node bifurcation separating monostable and bistable regions in the E/R_{ext} parameter plane. (SN = saddle-node bifurcation, c = cusp point). Adapted from Krischer, K., Nonlinear Dynamics in Electrochemical Systems. In: Advances in Electrochemical Science and Engineering, Volume 8. Edited by Alkire, R. C.³³

There is a different type of bifurcation that is called Hopf bifurcation (HB)⁴⁸. In the HB the stability of a steady state is modified and a limit cycle or a periodic orbit is born, this is, oscillations are observed in these conditions.³³ A limit cycle can be defined as an isolated closed trajectory. The term isolated means that neighboring trajectories are not closed, they are

attracted or repelled from the bifurcation point. If all neighboring trajectories approach the limit cycle, it is called a stable limit cycle, otherwise, it is classified as unstable.⁴⁸

For small values of in series resistance, the system is monostable, and the polarization I/φ curve has the N-shape. The HB point is crossed twice at intermediate values of the series resistance, that are necessarily higher than the critical resistance value, R_{crit} , when the applied potential, E , is increased.³³ The unstable steady-state in the HB always lies on the NDR branch, resulting in a hysteresis in the cyclic voltammogram. The HB ends at some intermediate values of R_{ext} , therefore, oscillations do not exist under galvanostatic regime (that can be considered as a potentiostatic regime with infinite resistance), under which the system exhibits BS.

The two bifurcations can be distinguished employing impedance spectroscopy analysis.³³ The mathematical analysis are described in details by Koper,³⁰ but they can be summarized for potential control as:

- a SN bifurcation occurs when $Z(\omega = 0) = 0$;
- a HB happens if $Z(\omega \neq 0) = 0$.⁴⁹

The emergence of BS has been observed in different electrochemical systems, such as: the electroreduction of complexes of Ni(II) at a streaming mercury electrode⁵⁰⁻⁵³ in the electroreduction Hg(I)/Hg(II) ions coupled with convection⁵⁴, in the anodic dissolution of vanadium electrodes in acidic media^{55,56}, in the electro-oxidation of small organic molecules,⁵⁷⁻⁵⁹ and so forth. Overall, oscillations can appear along the BS region depending on the controlling parameters. Although, detecting more than two branches in electrochemical systems are very rare, tristability has been observed as well.^{52,60-62}

Considering the requirements to obtain a NDR, Nakanishi *et al.*⁶³ have demonstrated that additions of small amounts of 1,10-phenatrolin (phen) in the cathodic deposition of Cu^0 in acidic media can easily induce potential and current oscillations. His study extended the previous work of Schlitter *et al.*⁶⁴ which was the first one to report potential oscillations in copper and phen system, back in 1968. Nakanishi's paper proposes a mechanism for the electrochemical oscillations, and, in short, the autocatalytic variable was recognized as being the effective area of the electrode surface. Acidic solutions with different pH were used, and it was observed that the current suppression becomes more prominent as the solution becomes more acidic.⁶³ Although the adsorption effect of the protonated phen molecule is stated as the main cause of the current decrease, it is not considered the reason of the emergence of

the NDR. A two-step reduction reaction of bivalent ions copper is suggested, whereas the formation and adsorption on the metallic complex $[\text{Cu}(\text{phen})_2]^+$ is considered as the promoter of the NDR phenomenon. Cross-section images of the obtained deposit in potential oscillations displays a layered structure, in which the number of layers is equivalent to the number of the oscillation periods in the electrochemical experiment.

To the best of our knowledge, these are the only two references dedicated to the investigation of dynamic instabilities in this system. Herein, we report the presence of BS in the electrodeposition of Cu generated by the addition of phen in the reaction acid media. The gravimetric *in-situ* experiments aims to detect and disclose what are the major species adsorbed at the electrode surface during the nonlinear phenomena, whereas the impedance spectroscopy is destined to confirm the HN-NDR pointed out by Nakanishi.⁶³

1.3. Effect of organic molecules in electrodeposition systems

Since the 1,10-phenanthroline is the major specie that affect the electrochemical dynamic in the experiment it is essential to dedicate a section to unfold its chemical and electrochemical properties and major aspects. Firstly, phen is a heterocyclic organic compound containing two nitrogen atoms, as we can see in **Figure 3**, it is a white solid that is poorly soluble in aqueous media. Although its solubility increases in acidic media, the specie still shows low solubility and that is the reason why such low concentrations are used in our experiments. Phen is worldwide known in coordination chemistry, it forms strong chelates complexes with metal ions, such as copper, iron, nickel, ruthenium and gold, for instance.⁶⁵

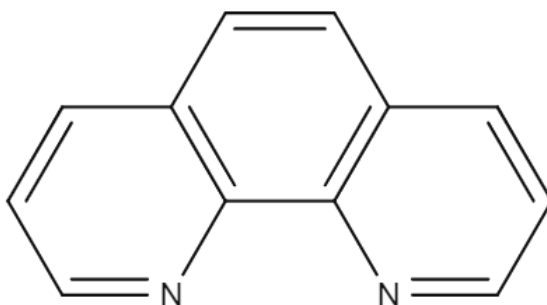
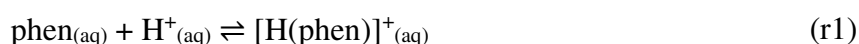


Figure 3: Structural representation of 1,10-phenanthroline.

Phenanthroline is categorized as chelate since it is a bidentate ligand capable of coordination to metal ion centers through the two nitrogen atoms.⁶⁵ Unlike bipyridine, which is also a well-known ligand in coordination chemistry, phen is a rigid ligand where the pyridyl groups are connected through an aromatic system.⁶⁶ The phen molecule is a weak base in aqueous solutions, since the pK_a is 5.12,⁶⁷ the protonation reactions occurs as following (r1):



Mitchell⁶⁸ suggested that a further reaction can occur in acid media, a self-stacking of the phen molecules, forming $[\text{H(phen)}_2]^+$ (r2), the calculated stability constant of the reaction is 2.11 in log units.



This fact agrees with the poor electron property of the heteroaromatic rings that leads to the lower donor ability of its nitrogen atoms.⁶⁹ Octahedral complexes of the type $\text{M(phen)(H}_2\text{O)}_4]^{2+}$, $[\text{M(phen)}_2(\text{H}_2\text{O)}_2]^{2+}$ and $[\text{M(phen)}_3]^{2+}$ are also found in aqueous media in which the metallic center ions is from the first-row of the transition metal block. The structural factors such as planarity, rigidity and hydrophobicity of phen are responsible for the high stability of the metallic complexes.⁶⁹

Phen molecules also shown strong interactions with metallic surfaces, in fact nitrogen-containing organic heterocycles can be used as additives in metal plating process and corrosion inhibition.^{70,71} In sum, the organic molecules act as a inhibitor in the electrode reaction, as a catalyst, this is, they do not take part in the reaction, they act only as regulators, controlling the rate of electrodeposition.⁷¹ Sugimasa *et al.*⁷⁰ investigated with *in-situ* scanning tunneling microscopy the adsorption of phen molecules in monocrystal copper surfaces with (111) crystalline orientation, in different potentials. It was observed polymer-like chains with phen molecules vertically orientated, where the nitrogens atoms faced the Cu(111) surface. The adlayer is stable in more positive potentials, whereas the phen molecules domains changes their size and orientation in more negative potentials, which evidence the potential-dependent orientation of the organic molecule.

Despite the $[\text{Cu(phen)}_2]^+$ not being luminescent in aqueous solutions, substituted phenanthrolines are extensively explored as a coordination ligand that can form metallic complex with luminescent characteristics. A relevant feature of the so-called $[\text{Cu(NN)}_2]^+$,

where NN stands for the substituted phenanthrolines, is the wide range of attainable modulation of their absorption and luminescence properties, which are related to structural factors.⁷² These facts establish the possibility of using phenanthrolines, *e.g.* molecules from the family of phen, in light sensitive reactions.

2. Objectives

This dissertation aims to provide a detailed study of the induced bistability in the electrodeposition of copper when 1,10-phenantroline is presented in an acidic environment. The knowledge of the reaction mechanism and of the properties around the processes that occur in the electrode/solution interface can provide a better understanding about the phenomenon and may enable a fuller comprehension of the system dynamics. The investigation disposed here is devoted to a deep understanding of the kinetics underlying the nonlinear behavior and a mechanistic interpretation concerning the bistability phenomena is provided. For the purpose of identifying the major adsorbents species involved in the reactions that take place in the electrode interface mass variations detections are obtained through experiments using the Electrochemical Quartz Crystal Nanobalance.

3. Methodology

3.1. Electrochemical system

Figure 4 exhibit a scheme of the electrochemical cell used in the experiments. The electrochemical experiments were carried out using as the counter electrode (CE) a high area platinized-platinum foil, as the Reference Electrode (RE) a Reversible Hydrogen Electrode (RHE) and as the Working Electrode (WE) a polycrystalline platinum sheet with an electrochemical area of 1.4 cm^2 inferred by the charge in the hydrogen Under Potential Deposition.⁶³ All glasses apparatus and also the metallic electrodes were cleaned by the immersion in sulfonitric solution overnight for at least 12 hours, period that was more than enough to guarantee the oxidation of organic impurities and metallic residues that might be present in the cell and at the electrodes surfaces. After, exhaustive rinses were made in all apparatus and, at least, one boil with ultrapure water (Milli-Q Millipore, $18.2 \text{ M}\Omega \text{ cm}$) were done in glasses devices, boiling in Milli-Q allows the dissolution of ions that can be possibly adsorbed at the glasses apparatus.

Before each experiment the electrochemical cleaning procedure of the platinum WE was performed by doing cyclic voltammeteries at the scan rate of 1.0 V s^{-1} in the potential interval from 0.05 to 1.30 V for about 500 times in order to assure a reproducible surface structure. The cleanness of the apparatus was checked from successive cyclic voltammograms at 0.05 V s^{-1} in the same potential window until the characteristic voltammetric profile for polycrystalline electrode was observed. The supporting electrolyte used for the electrochemical cleaning and for obtaining the characteristic voltammetric profile was 0.5 mol L^{-1} of H_2SO_4 (Sigma-Aldrich, $\geq 95\text{-}98 \%$). The supporting electrolyte for copper electrodeposition was prepared from H_2SO_4 and CuSO_4 (Sigma-Aldrich, $\geq 98 \%$) solutions using ultrapure water (Milli-Q) with final concentrations of 0.5 mol L^{-1} each. The surface inhibition was induced by the addition of 1,10-phenanthroline (Sigma-Aldrich, $\geq 99 \%$) in the reaction media, with final concentrations of 0.5, 1.0, 1.5 and 2.0 mmol L^{-1} .

Before the experiments, the electrolyte was kept in an ultrasonic bath for, at least, 10 minutes in order to obtain a better dissolution of phen. Subsequently, the solution cell was purged for a minimum of 15 minutes with molecular nitrogen (White Martins, 99.99%) and maintained under closed inert atmosphere to avoid the presence of molecular oxygen. The electrochemical system was controlled with a potentiostat (Autolab/Eco-Chemie,

PGSTAT302N) equipped with SCAN250, FRA32M and EQCM-oscillator modules in all electrochemical experiments, such as the cyclic voltammetries, the impedance spectroscopy and the gravimetric measurements. All experiments were carried out at room temperature.

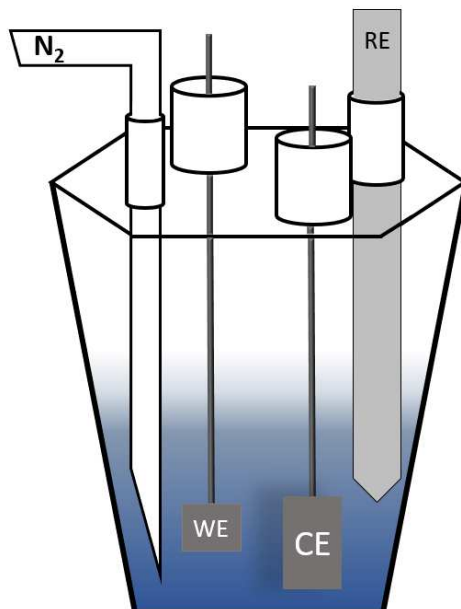


Figure 4: Scheme of a three-array electrochemical cell with the Work Electrode (WE), Counter Electrode (CE) and Reference Electrode (RE).

3.1.1. Cyclic voltammetries

The Upper and Lower potentials applied in the cyclic voltammetries are specified in each graph and unless stated otherwise the scan rate (dE/dt) is 0.01 V s^{-1} , this scan rate is sufficiently small at this system to guarantee a quasi-stationary state. **Figure 5** display a scheme of the cyclic voltammetry experiment, indicating the Start, Upper and Lower Potential and also the slope dE/dt . When specified the external resistance, R_{ext} , is connected in series to the WE through a resistance decade box.

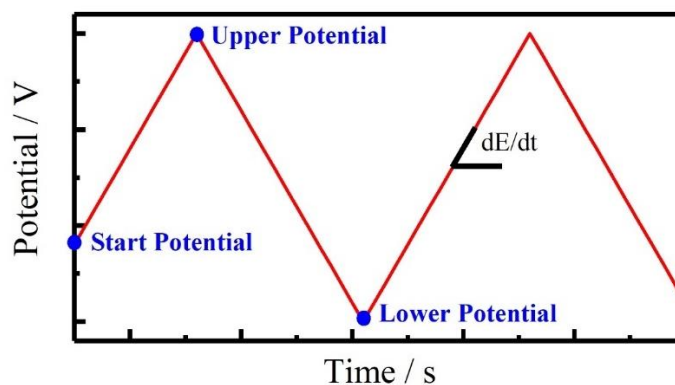


Figure 5: Scheme of a cyclic voltammetry showing the Start Potential, the Upper Potential and the Lower Potential. The slope corresponds to the scan rate, dE/dt of the cyclic voltammetry.

3.1.2. Electrochemical Impedance Spectroscopy

The Electrochemical Impedance Spectroscopy (EIS) is powerful analysis technique, employed to detect modifications in the interfacial properties of the electrode during an electrochemical process. The EIS technique can be useful for the stabilities analysis of the electrochemical systems, including the diagnosis of the type of bifurcation and also the class of NDR.¹² In the EIS experiment the electrochemical cell is first brought into a steady-state, or at least, a quasi-steady-state, as in our case. The desired quasi-stationary potential was applied for 300 s. Then, the system is perturbed with an applied *ac* voltage, in our case. An alternated current be applied as well. Typically, the alternated potential has sinusoidal form, in our experiments the sinusoidal potential perturbation was carried out at the frequency range of 50 kHz to 0.5 mHz and with amplitude of ± 10 mV. The EIS experiments were conducted around the steady-state potentials of 0.24, 0.12 and -0.05 V. The frequencies of perturbation were applied decreasing the frequency, using a logarithmic frequency step type, acquiring 50 point per experiment.

3.1.3. Electrochemical Quartz Crystal Nanobalance

The Electrochemical Quartz Crystal Nanobalance (EQCN) is an *in-situ* method exploited in the study of electrochemical reactions. It allows the detection of mass changes at a metal coated quartz resonator immersed in electrolyte during electrochemical experiments.⁶³ The mass variations can be associated with different process, such as deposition or dissolution

of a film, ions and/or solvents exchange between film and electrolyte, among others. The variations in the frequency of perturbation of the piezoelectric material are detected when a mass variation process occurs in the surface of the material. The frequency and mass variation are correlated by the Sauerbrey equation, Eq. 12.⁷³

$$\Delta f = - \frac{2f_o^2}{A \sqrt{\mu_c \rho_c}} \Delta m = - \kappa \Delta m \quad \text{Eq. 12}$$

In which Δf is resonating frequency variation in Hz, f_o is fundamental quartz crystal frequency, A is the piezoelectrically active area, μ_c is the shear modulus of the AT-cut quartz, ρ_c is the quartz density and Δm is the mass change.⁷³ The constant κ in the right is the experimental calibration constant, used for converting the Δf into Δm . The calibration constant is obtained using a well-known electrochemical reaction, in our case, the electroreduction of Cu^{2+} in acid media, in a two-electron transfer process (r3):⁷⁴



From the charge density (ΔQ) involved in the electroreduction of copper ions at a constant current, I , during a time interval, Δt , the areal density of mass of the copper deposit is obtained from Eq. 13:

$$\Delta m = \frac{MM}{zF} \Delta Q = \frac{MM}{zF} I \Delta t \quad \text{Eq. 13}$$

Where MM is the molar mass of copper (63.5 g mol^{-1}), z is the electrovalence of copper ions, +2, and F is the Faraday constant. The calibration constant, κ , can be calculated combining Eq. 12 and Eq. 13:

$$\kappa = - \frac{F}{MM} \frac{\Delta m}{I \Delta t} \quad \text{Eq. 14}$$

The value of $-5.816 \cdot 10^{-9} \text{ g Hz}^{-1}$ was determined as the calibration constant for our system. Thereby, mass changes during electrolysis can be obtained from Δf vs E curves, while mass/charge ratios can be evaluated from the slope of the Δm vs q (charge density) curves.⁷³ In the EQCN experiments, the WE used was a disk shaped quartz crystal 5 MHz AT cut, consisting

of a Au film evaporated over a thin Ti layer - Ti/Au polished with a geometric area of 0.385 cm².

3.2. Imaging Analysis

Surface images were obtained using a Scanning Electron Microscope (SEM) (Quanta FEG 250 FEI) operating at 20 kV. For each sample, the potential of the electrode was cycled 20 times in the potential from -0.1 to 0.3 V at $dE/dt = 0.01 \text{ V s}^{-1}$. The scan rate used is identical to the one used in the others electrochemical experiments. Afterwards, when the analysis potential was reached, the WE was removed from the cell for the microscopy analysis. The images taken in the SEM contain information about the topological structure of the copper deposit over the platinum electrode. During the 20 cyclic voltammeteries there is a continuous deposition of copper at the platinum surface. The copper layer obtained is so thick at this point that, in the 20th cycle, we can consider the copper electrodeposition takes place on a surface containing only copper.

4. Results and discussion

4.1. Cyclic voltammetries and bifurcation diagrams

First of all, in order to verify the cleanness of the cell and electrodes, a standard voltammetric profile of the platinum surface is obtained. The cyclic voltammetry acquire is presented in **Figure 6a**, the potential was swept between potentials of 0.05 V and 1.3 V vs RHE. Multiples scans are made until we reach a stable cyclic voltammetry, that is, the cyclic voltammetry scan profiles do not change from one cycle to the other, typically 10 cycles are used in order to meet these conditions. In fact, this procedure of only showing the stabilized cycle is carried out in all cyclic voltammetries from here on. The standard concentration of H_2SO_4 and scan rate used in this test are 0.5 mol L^{-1} and 0.05 V s^{-1} , respectively, which was used in our experiment. The pattern obtained confirms that our cleaning procedure is efficient, since the voltammogram portray coincides with the standards ones reported in the literature.⁷⁵

The profile displayed in **Figure 6a**, which we typically call platinum blank, can be fragmented in three regions. The first one begins at the potential of 0.05 and ends around 0.40 V and it is attributed to the hydrogen Under Potential Deposition. In the negative scan, this is, decreasing the potential, we observe negative current values, correlated to the adsorption and reduction of the H^+ , forming a Pt-H monolayer over the platinum surface. In the opposite scan, we slowly increase the potential and observe positive current values, now related to the desorption and oxidation of hydrogen species presented on the electrode surface.⁷⁶

Moving on, between the potentials of 0.40 V and approximately 0.60 V we see what is called electric double-layer domain. It is characterized for the absence of any electron transfer phenomenon, this is, there is no faradaic process in this region. The small current value detected in this potential window is attributed to the electrical double layer charging, correlated to a capacitive component of the system.⁷⁶ The last region starts at 0.60 V and ends up at 1.3 V, it is known as the surface oxide formation/reduction domain. In the positive scan, the faradaic processes are linked to the adsorption and oxidation of water molecules at the platinum surface, forming platinum oxides species, termed Pt-O. These species are reduced in the negative scan, in a reverse electro reaction, under which negative current values are recorded.

It is very important reiterate that in potentials smaller than 0.05 V, the major faradaic process that occur in these experimental conditions is the hydrogen evolution, this is, the desorption of the Pt-H species towards the formation of H_2 . In higher potentials, greater than

1.5 V, the molecular oxygen evolution takes place. In a similar way, Pt-O species leads the formation of O₂.⁷⁶

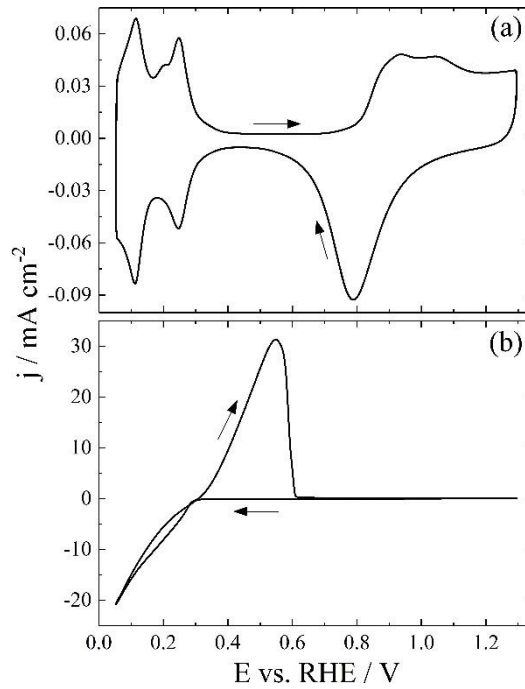


Figure 6: (a) Cyclic voltammograms of the Pt|H₂SO₄ system at $dE/dt = 0.05 \text{ V s}^{-1}$ in the potential window: (a) 0.05 to 1.30 V. (b) Same as item (a) but with scan rate of 0.01 V s^{-1} and with the addition CuSO₄. [H₂SO₄] = 0.5 mol L^{-1} and [CuSO₄] = 0.5 mol L^{-1} . The arrows indicate the sweep direction.

The charge due to the oxidation of adsorbed hydrogen, Q_{ox}^H , obtained by integration of the area under the current curve in the hydrogen desorption domain, is correlated to the electrochemically active surface area, $ECSA$, through Eq. 15:

$$ECSA = \frac{Q_{ox}^H}{\nu \times c} \quad \text{Eq. 15}$$

In which ν stands for the scan rate used in the experiments and c corresponds to charge oxidation of a monolayer of adsorbed hydrogen per unit area, which is equivalent to $210 \mu\text{C cm}^{-2}$ for the polycrystalline platinum. The $ECSA$ is used to convert all the currents values in the cyclic voltammeteries, in current densities values. Although the surface area changes continuously during the electrodeposition process, the current values are always normalized with respect to the initial active area value of the platinum surface.

Figure 6b depicts cyclic voltammograms at slow sweep rates, $dE/dt = 0.01 \text{ V s}^{-1}$, of copper sulfate in sulfuric acid solution with final concentration of 0.5 mol L^{-1} for each reagent. The potential window is the same that in **Figure 6a**, this is, 0.05 to 1.30 V. The first thing to note is the change in order of magnitude of the detected current values, the current densities that before, were not bigger than 0.1 mA cm^{-2} now assumes values up to 30 mA cm^{-2} .

The electrodeposition of Cu is a well-known reaction studied along several decades.⁷⁷⁻⁸¹ As already reported in an acidic media,⁷⁸ the reduction of Cu takes place around 0.30 V and continues in lower potentials, following an instantaneous nucleation mechanism at very first stage of the faradaic reaction for higher concentrations of copper (0.025 and 0.05 mol L^{-1}). The current density reaches -20 mA cm^{-2} at 0.05 V and still shows negative values of currents up to the crossover potential of 0.30 V. From this potential, in the positive direction, it is possible to observe an intense current density peak of 32 mA cm^{-2} at 0.55 V, corresponding to the oxidation of the Cu deposits and, in sequence, falling down to zero current. For $E > 0.62 \text{ V}$ Cu dissolution and a surface passivation occur.

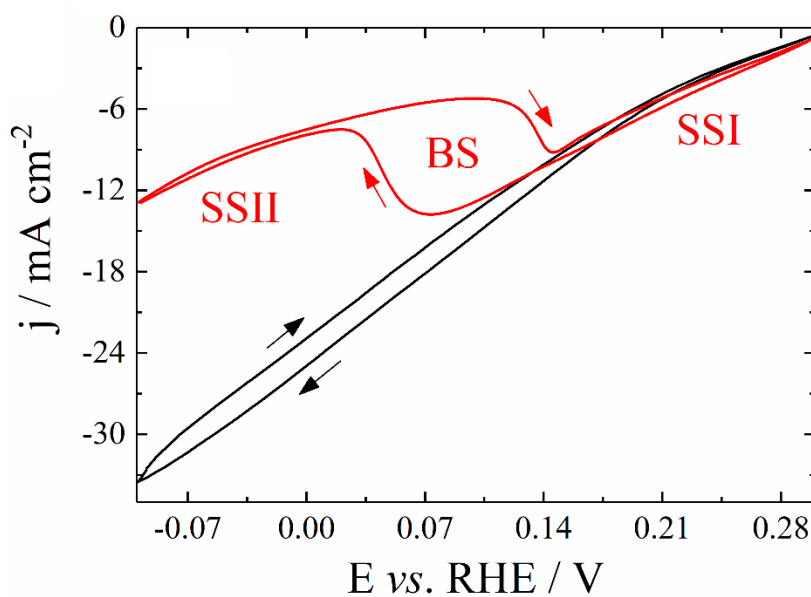


Figure 7: Cyclic voltammograms of the Pt|H₂SO₄,CuSO₄ system at $dE/dt = 0.01 \text{ V s}^{-1}$ in the potential window: -0.10 to 0.30 V (black line); but with addition of 2.0 mmol L^{-1} of phen (red line). [H₂SO₄] = 0.5 mol L^{-1} and [CuSO₄] = 0.5 mol L^{-1} . The arrows indicate the sweep direction.

In **Figure 7** we focus on the potential window from -0.10 to 0.30 V in the same electrolyte concentrations as in **Figure 6b** (**Figure 7**, black line), and, after the addition of 2.0 mmol L⁻¹ of phen, -0.10 to 0.30 V (**Figure 7**, red line). In this potential domain, the electrodeposition of Cu takes place continuously (black line) with a small hysteresis along the positive and negative sweeps. There is a mean separation of 1.9 mA cm⁻² between the curves. However, when phen molecules are added in the electrolyte, with final concentration of 2.0 mmol L⁻¹ (red line), the deposition process is substantially suppressed for $E < 0.15$ V. This inhibition reached a minimum value of -5.2 mA cm⁻² at 0.1 V and produced a noteworthy separation of 8.6 mA cm⁻² between the current curves along the both directions of the sweeps in the interval of 0.03 - 0.15 V. The suppression is more pronounced below 0.03 V, but it manifests slightly above 0.15 V as well. Nakanishi *et al.*⁶³ have postulated that adsorbed metallic complexes, [Cu(phen)₂]^{+(ad)}, could be mainly responsible for the inhibition and the formation of the NDR. Overall, for $E < 0.03$ V and $E > 0.15$ V the hysteresis is so small that can be considered negligible. Accordingly, we considered a BS domain around the interval of $0.03 \text{ V} < E < 0.15 \text{ V}$ and two steady states regions, one at $E > 0.15 \text{ V}$ (SSI: Steady State I) and another at $E < 0.03 \text{ V}$ (SSII: Steady State II).

It is important to note that the potential window of the BS domain do not depend on the vertex potentials in the cyclic voltammograms. As a matter of fact, cyclic voltammograms with different vertex potentials are displayed in **Figure 8**, the electrolyte conditions are the same as those used to obtain **Figure 7**: Cyclic voltammograms of the Pt|H₂SO₄,CuSO₄ system at $dE/dt = 0.01 \text{ V s}^{-1}$ in the potential window: -0.10 to 0.30 V (black line); but with addition of 2.0 mmol L⁻¹ of phen (red line). [H₂SO₄] = 0.5 mol L⁻¹ and [CuSO₄] = 0.5 mol L⁻¹. The arrows indicate the sweep direction.. Both upper and lower potentials were shifted. In **Figure 8a-c** the upper potential is increased in 0.1 V steps, from 0.2 V to 0.4, and indeed, the BS domain remains the potential window between 0 and 0.15 V. The lower potential is shifted as well, in **Figure 8d-f**, from 0 to -0.30 V, in the same potential step than before, and the same conclusion is obtained, there are no significant changes in the potentials of the BS domain.

At this point the experimental conditions where BS can be found were well determined. This knowledge allowed a safe variation in the controlling parameters without get too far from the BS domain. **Figure 9** shows the dependence of the upper and lower potential limits of the BS by the change of the R_{ext} (**Figure 9a-d**) at phen = 2.0 mmol L⁻¹ and the variation of concentration of phen in the reaction media (**Figure 9e-h**) at $R_{ext} = 28 \Omega \text{ cm}^2$. In this case, the external resistance is normalized by the electrode area factor, which is 1.4 cm², as stated

before. This is done so that our experiments can be compared if electrodes of different sizes are used.

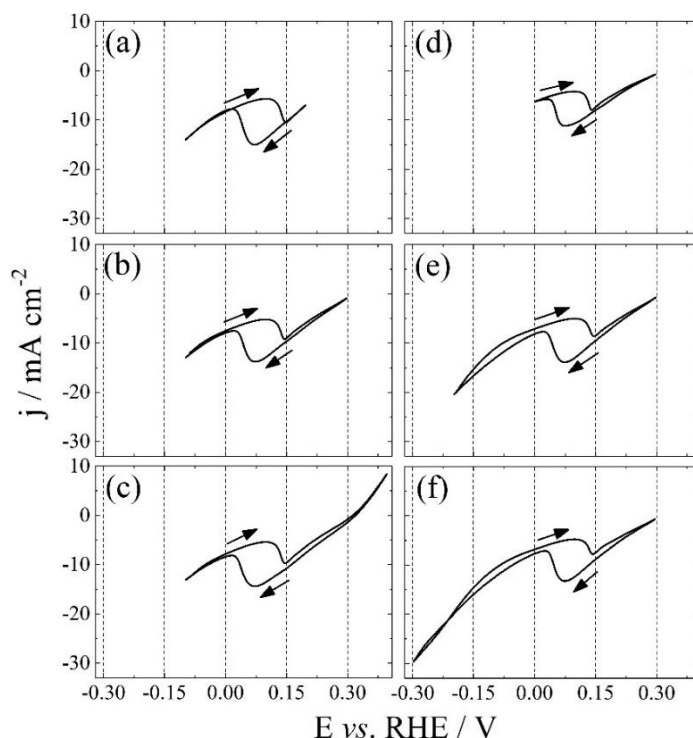


Figure 8: Cyclic voltammetry of the Pt|[H₂SO₄,CuSO₄,phen] system at $dE/dt = 0.01 \text{ V s}^{-1}$ in the potential window: (a) -0.10 to 0.20 V, (b) -0.10 to 0.30 V, (c) -0.10 to 0.40 V, (d) 0 to 0.30 V, (e) -0.20 to 0.30 V, (f) -0.30 to 0.30 V. [H₂SO₄] = 0.5 mol L⁻¹, [CuSO₄] = 0.5 mol L⁻¹ and [phen] = 2.0 mmol L⁻¹.

It is important to remember at this point the role of the external in series resistance in the electrochemical system. As previously stated, the equivalent resistance of the system, R , that includes both ohmic resistance, R_{Ω} , that is related to the electrolyte factors, and external resistance, R_{ext} , are decisive in determining whether or not dynamic instabilities will occur in the system, as explained in details in section 1.2. So, in order to meet the conditions of BS or other nonlinear phenomena, such as oscillations, the external resistance can be effortlessly altered in a decade resistance box.

All mapping experiments were conducted in low sweep rates of $dE/dt = 0.01 \text{ V s}^{-1}$. Similar observations were done using slow rates in the cyclic voltammetries by Orlik *et al.*⁵⁶ Both concentration and external resistance are considered as experimentally accessible

controlling parameters in electrochemical systems and can induce dynamic instabilities by subtle changes.²⁷

The increase of R_{ext} is followed by a progressive increase on the BS domain and it is also accompanied by a pronounced shift to negative potentials, as verified in **Figure 9a-d**. For external resistances of 7, 14, 21, 28 $\Omega \text{ cm}^2$, the difference between the upper and lower potential limits of the BS was found to be 0.10, 0.16, 0.21, 0.26 V, respectively (we adopted the turning points in the j vs E curves for the calculation). Indeed, the process that results in the abrupt current changes and generates the BS seems to occur in particular potentials values. This is a strong indicative that the adsorption of the inhibiting species happens in those specific potentials and remains on the surface, desorbing completely later on in the reverse cycle.

On the other hand, the increase of the concentration of phen resulted in a shrinkage of the BS domain. At the lowest employed concentration of phen (0.5 mmol L^{-1}), only the lower limit is observed, and an expressive hysteretic profile does not arise (**Figure 9e**). When the concentration of phen is increased to 1.0 mmol L^{-1} a different scenario appears, and the BS is clearly established under these conditions (**Figure 9f**). Note that the approximation of the upper and lower limits to an invariable potential became even more evident in larger concentrations of phen, that is, 1.5 mmol L^{-1} or 2.0 mmol L^{-1} (**Figure 9g-h**). No significant changes were observed between these two concentrations, which indicates a surface saturation over the copper deposit of the inhibiting species above of the concentration of 1.5 mmol L^{-1} .

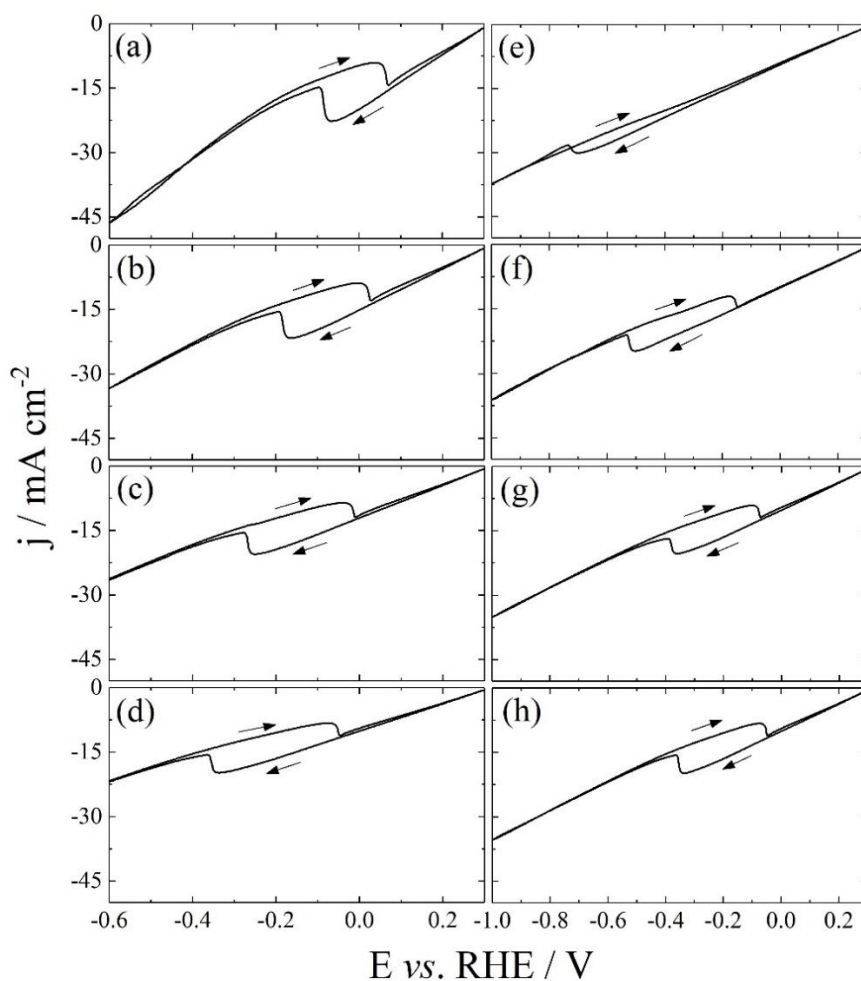


Figure 9: Cyclic voltammograms at $dE/dt = 0.01 \text{ V s}^{-1}$ under different external resistances at $\text{phen} = 2.0 \text{ mmol L}^{-1}$ and $R_{ext} =$ (a) 7, (b) 14, (c) 21, (d) $28 \Omega \text{ cm}^2$ and under the effect of the concentration of phen at $R_{ext} = 28 \Omega \text{ cm}^2$ and phen = (e) 0.5, (f) 1.0, (g) 1.5 and (h) 2.0 mmol L^{-1} . The arrows indicate the direction of the sweep.

A summary of the effect of R_{ext} and concentration of phen on the bistable behavior in the electrodeposition of Cu is showed in terms of a bifurcation diagram in **Figure 10**. At first glance, its shape has a considerable resemblance with the bifurcation diagrams of systems N-NDR.¹² In fact, Nakanishi *et al.*⁶³ have observed electrochemical oscillations in both current and potential which is a good indicative that the cathodic deposition of Cu perturbed with phen remains in the Hidden N-NDR (HN-NDR) subsystem, which means that possibly an intermediate blocks the surface and reduces the global rate in lower potentials.^{27,28}

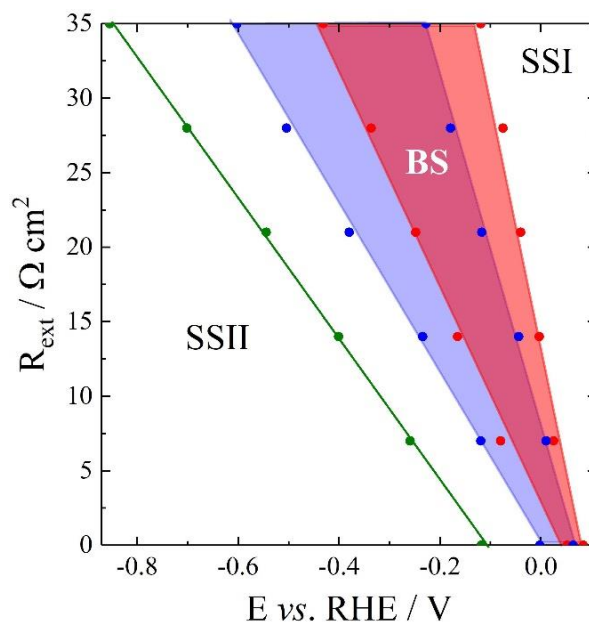


Figure 10: Bifurcation diagram R_{ext} vs E measured with $dE/dt = 0.01 \text{ V s}^{-1}$ in several concentrations of phen: 0.5 (green line), 1.0 (blue line), 2.0 mmol L^{-1} (red line).

Additionally, **Figure 10** highlights the SN bifurcation as the lines surrounding the domains of the BS and how it is strongly modified by the increase of the concentration of phen. A straight green line represents the slight suppression of the current when $[\text{phen}] = 0.5 \text{ mmol L}^{-1}$ is present in the electrolyte. The contraction of the BS domains reaches a maximum around 1.5 mmol L^{-1} and negligible changes are observed when compared to the domain formed at 2.0 mmol L^{-1} , this statement can be verified in **Figure 11**, as there are no significant difference between the evaluated bifurcation diagram of both concentrations.

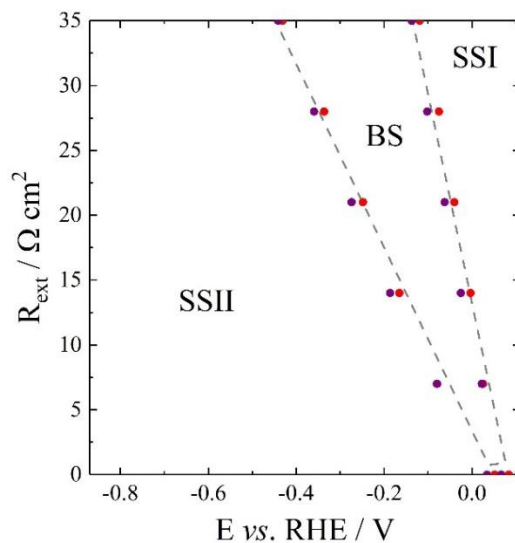


Figure 11: Bifurcation diagram R_{ext} vs E measured at sweep rate of $dE/dt = 0.01 \text{ V s}^{-1}$ in two concentrations of phen: 1.5 mmol L^{-1} (purple dots) and 2.0 mmol L^{-1} (red dots).

The calculated areas of the bifurcation diagrams in **Figure 10** are 7.9 and $6.3 \text{ V } \Omega \text{ cm}^2$ for 1.0 and 2.0 mmol L^{-1} of phen, represented in blue and pink, respectively. The bifurcation diagram of the concentrations of 1.0 and 2.0 mmol L^{-1} overlap in a region of intermediate potentials. The overlap is represented by the darker purple color, resulting from the mixture of blue and pink. The compression in the bifurcation diagram as the concentration of inhibiting species increases is in agreement with the numerical simulations performed by Nascimento *et al.*⁸² A considerable shrinkage of the Hopf domain was observed as the irreversible surface poisoning evolved. The dynamics changed accordingly, and the chaotic oscillations were dramatically suppressed.

4.2. Electrochemical Impedance Spectroscopy characterization

As discussed in details before in the section 1.2.1, the SN bifurcation can be confirmed by the EIS under potentiostatic control when the imaginary part of the impedance is zero as the frequency of perturbation tends to zero as well,⁸³ this is, $Im(Z(\omega = 0)) = 0$ for. From here on, the real component of the impedance is represented for simply $Z(\omega)$, and the imaginary part by $Z'(\omega)$. **Figure 12** depicts Nyquist plots, the real impedance component, $Z(\omega)$ vs the imaginary part, $Z'(\omega)$, of the electrodeposition of Cu in three different applied voltages of 0.24 , 0.12 and -0.05 V which are located at the SSI, the BS domain and the SSII, respectively. Black

lines indicate the cathodic reduction of Cu without the presence of phen, while in red lines, phen is present in the reaction media.

Figure 12a shows that the process has distinct time scales with the presence of two semicircles, one at high and another at low frequencies. They are related to two limiting steps which compete simultaneously and are affected by the applied voltage – high frequencies describe activation control, whereas low frequencies describe mass transport control.⁸⁴ In the latter, the Warburg impedance shows a decreasing imaginary component, resulting in the observed trend⁸⁵ (**Figure 12a**, black line). It has been also ascribed that low-frequency loops is strongly dependent of the growth mode of copper deposits.^{86,87} There are different interpretations for the inductive behavior in the lowest frequencies, but it can represent the adsorption-desorption of inhibiting species, for example, anions from the electrolyte⁸⁸ or a nucleation process^{86,87} (**Figure 12a**, black line). The ohmic drop, R_{Ω} , shows very low values of around $2.2 \Omega \text{ cm}^2$ in all experiments.

Interestingly, the first semicircle is not affected by the presence of the phen but causes a significant increase in the real and imaginary components of the low-frequency loop in the **Figure 12a**, red line. As the dominant loop belongs to higher frequencies spectrum, the global faradaic reaction is not highly affected by the phen molecules under the voltage of 0.24 V. The **Figure 7**, in the SSI, reflects this description where no significant suppression is observed with and without the presence of phen, in which close values of current density are observed, corroborates with this scenario. For the second process located in lower frequencies the size of the semicircle increases, reflecting the surface inhibiting effect of the phen (**Figure 12a**, red line).

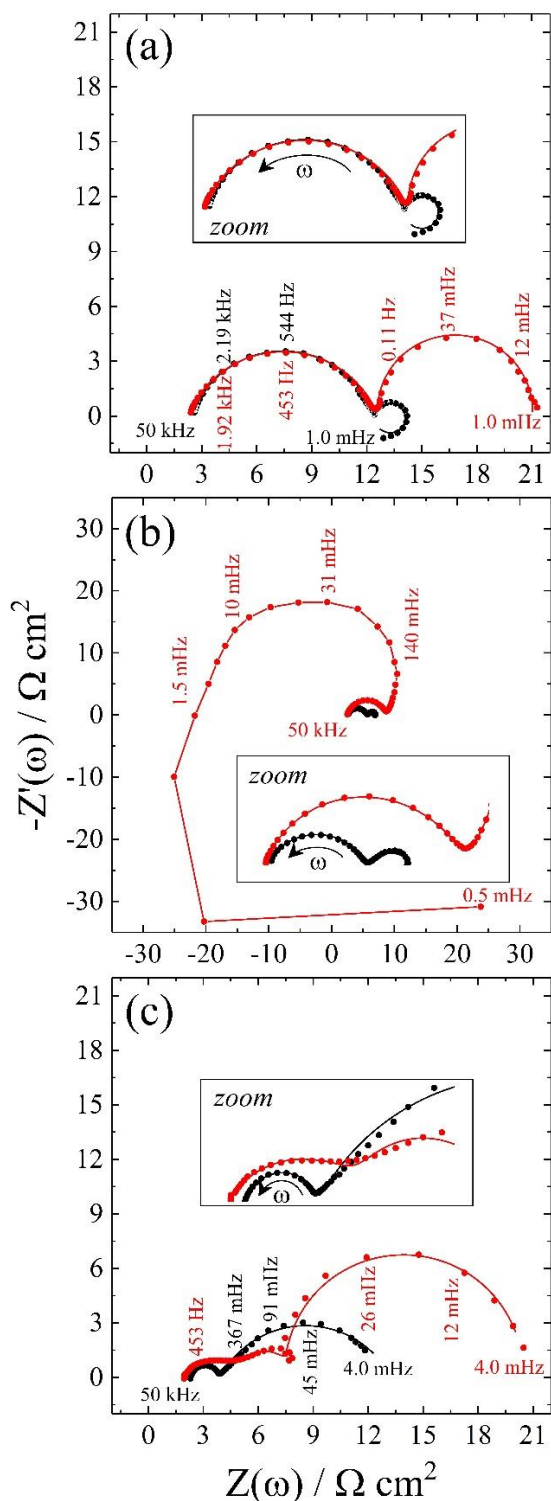


Figure 12: Nyquist plots for the electroreduction of Cu without (black lines) and with (red lines) phen molecules in the concentration of 2.0 mmol L^{-1} at the applied voltages: (a) 0.24, (b) 0.12 and (c) -0.05 V. The insets correspond to a “zoom in” on the plates a-c.

The dynamic instability induced by phen becomes even clearer in the **Figure 12b**. The first observation is the anticlockwise movement in lower frequencies on the Nyquist plot

and the subsequent intersection in the real axis at 1.5 mHz which is related to the Hopf bifurcation, that is, $Z'(\omega) = 0$ for $\omega \neq 0$, this is the imaginary component of the impedance is null (**Figure 12b**, red line). In fact, the hidden negative impedance ($Z'(\omega) < 0$ for $\omega \neq 0$) suggests that the system belongs to the HN-NDR class⁸³ and consequently confirms the proposition already discussed.⁶³ Accordingly, the autocatalytic evolution of the double layer potential is driven by surface area changes which makes a very easy handling of the BS domain by the control of the concentration of phen.

Figure 12c depicts an expressive decrease of the diameter of the high-frequency loop due to the fast charge of the copper ions on the surface in agreement with **Figure 7**, black line, in the SSII domain, where we observe an increase in the current density magnitude. As also expected, a mass transport limitation acts in this applied voltage and bigger semicircles can be observed in lower frequencies.⁸⁸ However, we believe that the presence of phen has a strong effect on the Cu deposits growth and the low-frequency loop is mainly attributed to the inhibition of the surface by adsorption processes related to the phen presence (**Figure 12c**, red line), which induces the decrease of the overall current (**Figure 7**, red line, SSII).

4.3. Gravimetric analysis

In this section we will provide further insights on the nature of the adsorbed species in the electrode surface during the electrochemical reaction. This will allow us to propose a mechanistic interpretation of how BS appears in this system. **Figure 13** shows the j vs E curves (dashed lines) during the electroreduction of Cu at $dE/dt = 0.02 \text{ V s}^{-1}$ followed by the corresponding mass changes profiles (full lines) obtained with the aid of the EQCN. In this case a higher scan rate was necessary since the detected mass variations were too small, therefore, they were in the detection limit of the EQCN used. A higher scan rate provides us larger currents values and consequently, an increase in the mass variation.

The system was perturbed with small additions of phen as final concentration of 0 (black), 0.5 (green), 1.0 (blue) and 2.0 mmol L⁻¹ (red). To study the BS domains by mass variation measurements (Δm), the potential window was 0 to 1.0 V in order to prevent the continuous accumulation of Cu on the surface by its dissolution in higher potentials and, then, preventing a monotonic ascending curve of Δm . The copper reduced in the potential range of 0 to 0.3 V is further oxidized in potentials larger than 0.3 V, from 0.3 to 1.0 V. Therefore, every

time the cycle is reestablished the copper deposition occurs over a platinum clean surface. For this reason, the mass changes profiles were normalized to zero at $E = 1.0$ V. As before in the cyclic voltammetries, just one voltammogram and one correlated mass variation curve is displayed in **Figure 13**: Current densities (dashed line) and mass variations (full line) at $dE/dt = 0.02$ V s⁻¹ with additions of phen as final concentration of (a) 0 (black), (b) 0.5 (green), (c) 1.0 (blue), (d) 2.0 mmol L⁻¹ (red). [H₂SO₄] = 0.5 mol L⁻¹ and [CuSO₄] = 0.5 mol L⁻¹. The arrows indicate the direction of the sweep..

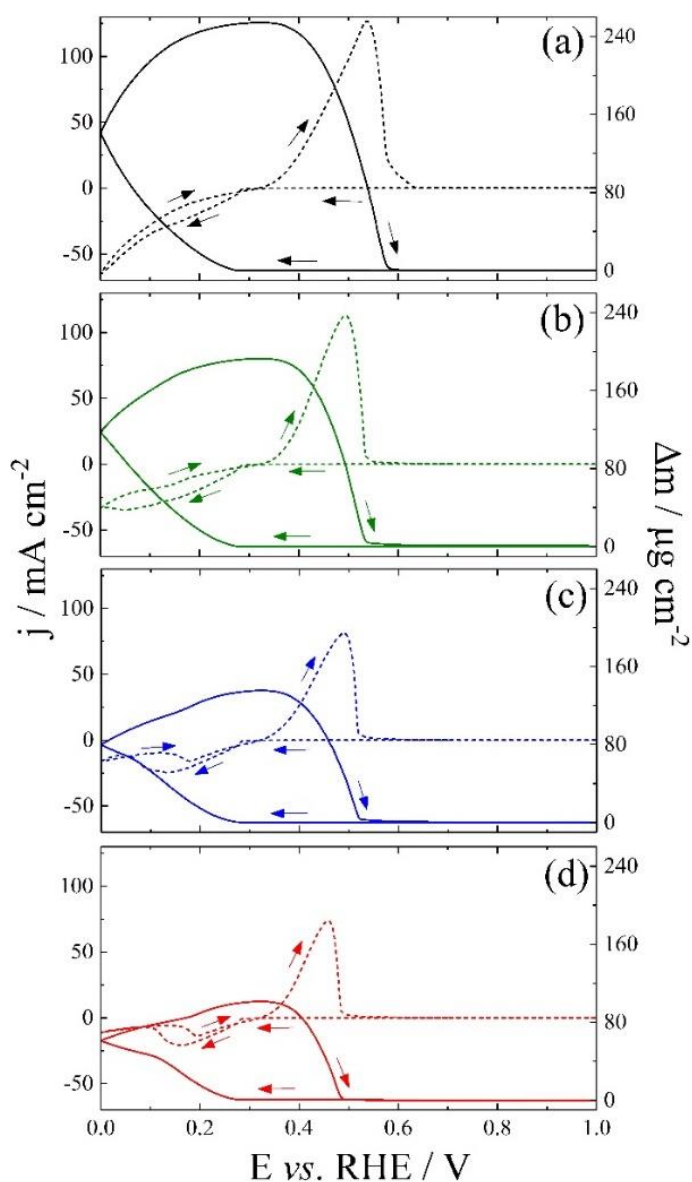


Figure 13: Current densities (dashed line) and mass variations (full line) at $dE/dt = 0.02$ V s⁻¹ with additions of phen as final concentration of (a) 0 (black), (b) 0.5 (green), (c) 1.0 (blue), (d) 2.0 mmol L⁻¹ (red). [H₂SO₄] = 0.5 mol L⁻¹ and [CuSO₄] = 0.5 mol L⁻¹. The arrows indicate the direction of the sweep.

As observed in **Figure 13** the crossover potential is 0.3 V but a significant deposition of Cu occurs only for $E < 0.26$ V and begins to decay around $E > 0.35$ V in the positive direction. The removal of deposited Cu is dependent on the concentration of phen. As it increases, the suppression of the global rate can be evidenced by the decrease of the oxidative and reductive currents followed by reduction of the corresponding mass changes profiles in the positive and negative sweeps, respectively. At zero concentration of phen, the mass variation goes as high as $240 \mu\text{g cm}^{-2}$, whereas, when 2.0 mmol L^{-1} of phen is present in the reaction media, the largest assumed Δm is around $100 \mu\text{g cm}^{-2}$.

Interestingly, an expressive variation of the mass can be observed in the lower and upper potential limits of the BS domains, where the curve Δm vs E flips the concavity and bends, forming a considerable angle especially at higher concentrations of phen. This observation suggests that there is a strong adsorption of species dissolved in the electrolyte during the negative sweep. This abrupt current suppression is detailed in **Figure 14**. On the left we have the cathodic sweep of the cyclic voltammetry in the potentials between 0 and 0.2 V and on the right the respective curves of mass variation, Δm vs q . The gray highlighted areas represent the potential window where mass/charge ratios were calculated for the curves containing phen, they lay on at the domain with higher slope. When it is turned to positive direction, the adsorbed species are released from the surface and the copper deposition occurs quicker.

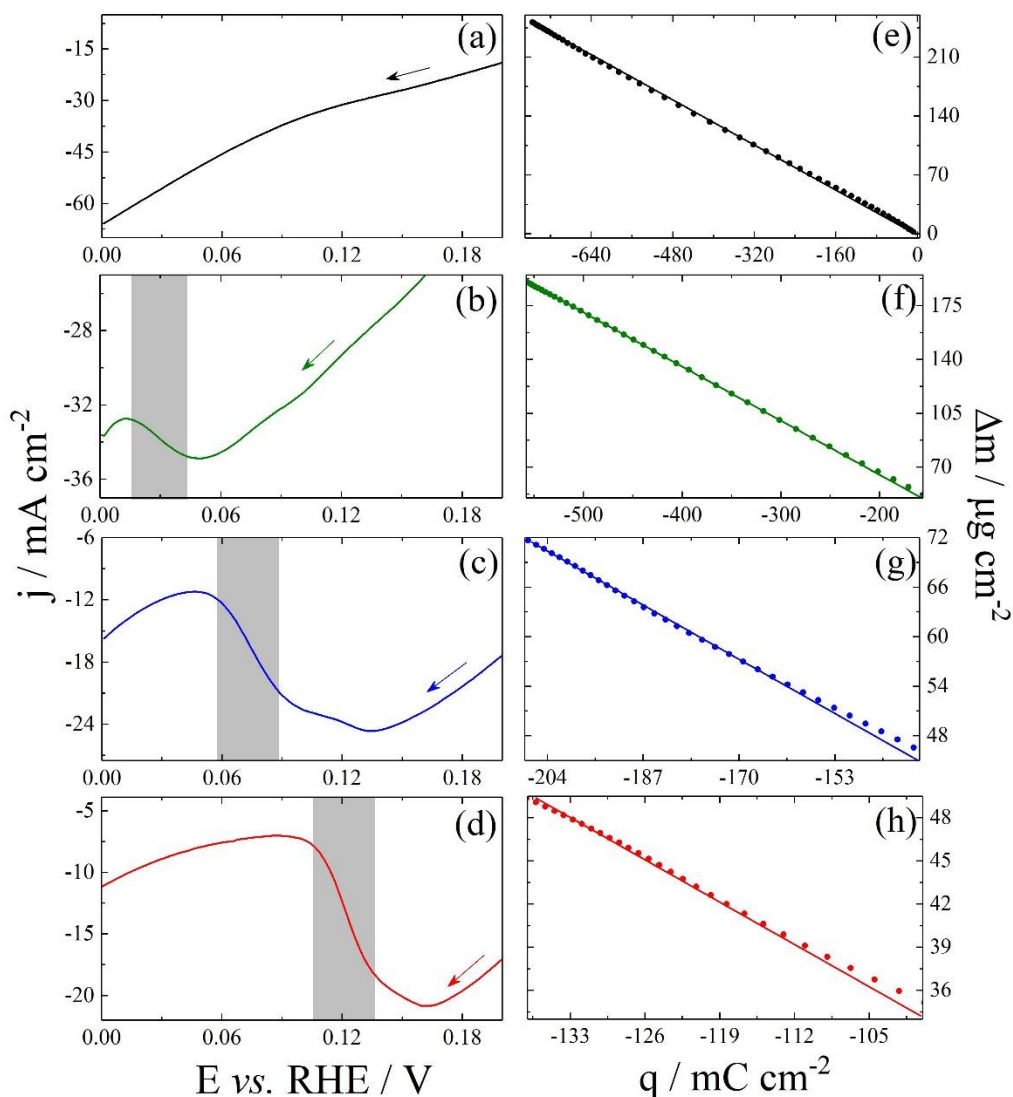


Figure 14: (a-d) j vs E and (e-h) Δm vs q in the potential interval of 0 to 0.20 V. The arrows indicate the direction of the sweep. The curves follow the color code used in the text for phen concentrations: 0 (black), 0.5 (green), 1.0 (blue) and 2.0 mmol L^{-1} (red). The gray bands represent the potential window where mass/charge ratios were calculated.

Focusing on the potential interval of 0 to 0.20 V, it was possible to calculate the mass/charge (m/z) ratios from j vs E and Δm vs E curves in the negative sweep as represented by the arrows. The colors assignments are the same of the **Figure 13**. The experimental m/z ratio is obtained from the slope of the linear fit of the Δm vs q curve. For the electrodeposition of Cu without the presence of phen (**Figure 14a,e**) it is equal to $332 \mu\text{g C}^{-1}$ which agrees with the theoretical value of $329 \mu\text{g C}^{-1}$ and retracts the electroreduction of Cu^{2+} to Cu^0 in a two-

electron reaction. In this calculation we used the molar mass of 63.5 g mol^{-1} for Cu and 2 electrons for the faradaic reaction, that is,

$$m/z = \frac{63.5 \text{ g mol}^{-1}}{2 \times 96485 \text{ C mol}^{-1}} = 329 \mu\text{g C}^{-1} \quad \text{Eq. 16}$$

As long as the phen concentration increases the m/z values increases as well. In this respect, we can safely consider that the process attributed to the adsorption, responsible to generate the instability in the negative sweep, takes place more intensely following the ascending order: $[\text{phen}] = 0.5 \text{ mmol L}^{-1}$ and $352 \mu\text{g C}^{-1}$ (**Figure 14b,f**), $[\text{phen}] = 1.0 \text{ mmol L}^{-1}$ and $392 \mu\text{g C}^{-1}$ (**Figure 14c,g**), $[\text{phen}] = 2.0 \text{ mmol L}^{-1}$ and $416 \mu\text{g C}^{-1}$ (**Figure 14d,h**). In that matter we can affirm that the adsorbent species acts more expressively as the concentration of phen is increased, this can both verified from the decrease in the density current values and the increase of mass variation.

Nakanishi *et al.*⁶³ have postulated that reduced form of the adsorbed metallic complexes, $[\text{Cu}(\text{phen})_2]_{(\text{ad})}^+$, could be the responsible for the inhibition effect, but in fact the complex $[\text{Cu}(\text{phen})_2]^{2+}$ is observed mainly in neutral media.⁸⁹ In acidic environment the ligands could be totally protonated which would weaken the coordination bonds between Cu^{2+} and phen and, therefore, generate uncoordinated ligands molecules. This is, de coordination is unfavored in more acidic media, so the formation of both $[\text{Cu}(\text{phen})_2]^{2+}$ and $[\text{Cu}(\text{phen})_2]_{(\text{ad})}^+$ is very unlikely in the environment of our experiments. According to this description, phen might also participate in the adsorption process causing the inhibition effect simultaneously with the adsorption of the metallic complexes.⁹⁰

The effect of adsorption of protonated phen over a copper surface was studied separately, vide **Figure 15**. First, a thick deposit of copper was made, through electrodeposition over the WE used in the EQCN experiments. Then, the cyclic voltammetries and mass variations were evaluated in an electrolyte containing only H_2SO_4 and phen, the system can be labeled as being $\text{Cu}|\text{H}_2\text{SO}_4, \text{phen}$, with different concentrations of phen. In this potential region, from 0 to 0.2 V, there is no Cu dissolution and the anodic and cathodic currents can be associated with desorption and adsorption processes, respectively, and larges currents are observed in higher concentrations of phen. The non-dissolution of copper in this potential window can be attested in **Figure 16**, black line, for the system containing as the WE a surface covered of copper and as the electrolyte 0.5 mol L^{-1} of H_2SO_4 , indeed is not observed for these

experimental conditions positive current values, which would be linked to oxidation processes. When 1.5 mmol L^{-1} of phen is added to this solution **Figure 16** black line, the detected current can be associated to adsorption/desorption process of the phen molecule.

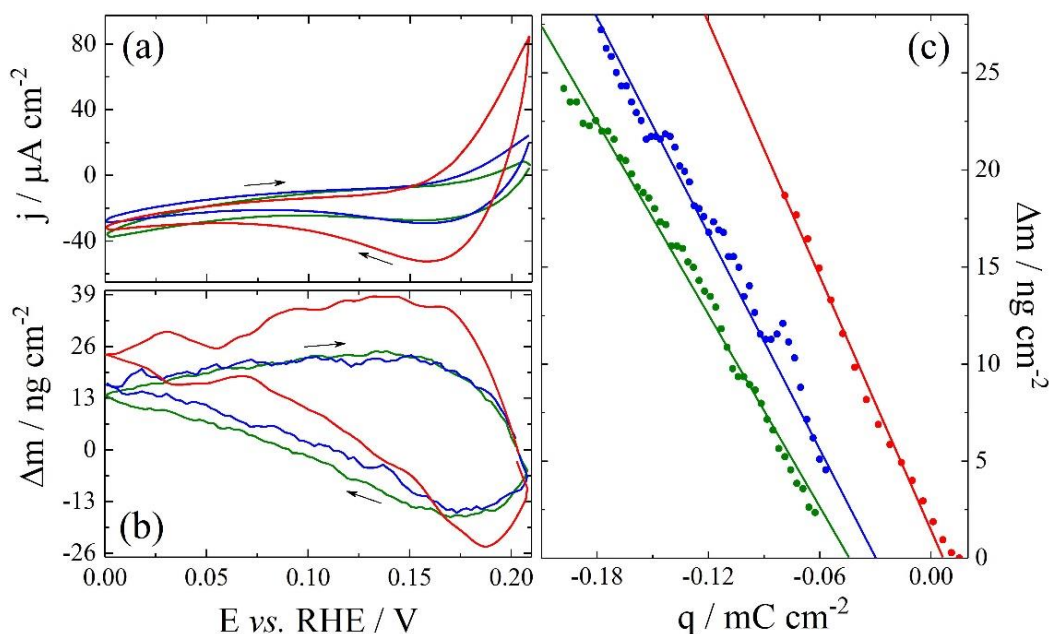


Figure 15: (a) j vs E , (b) Δm vs E , (c) Δm vs q in the potential interval of 0-0.20 V in the absence of CuSO_4 . The curves follow the color code used as previously: 0.5 (green), 1.0 (blue) and 2.0 mmol L^{-1} (red). $[\text{H}_2\text{SO}_4] = 0.5 \text{ mol L}^{-1}$.

Figure 15b shows that the respective mass profiles corroborate with the processes discussed previously. Note, however, that the mass scale is now in nanograms. In the positive sweep, the mass variations decrease for $E > 0.17 \text{ V}$ and increase in the negative sweep starting at $E < 0.19 \text{ V}$. In this respect, one can conclude that in NDR region observed during copper electrodeposition, the phen molecules (or their protonated form) interact with the surface competing for adsorption sites. We have tried to explain the nature of phen adsorbate by m/z ratios in the potential interval of 0.07 to 0.15 V, of the negative scan, the mass variations vs charge curves are displayed **Figure 15c**. Straight lines with a good fit were obtained and the slopes correspond to 166 (green line), 170 (blue line) and 181 $\mu\text{g C}^{-1}$ (red line).

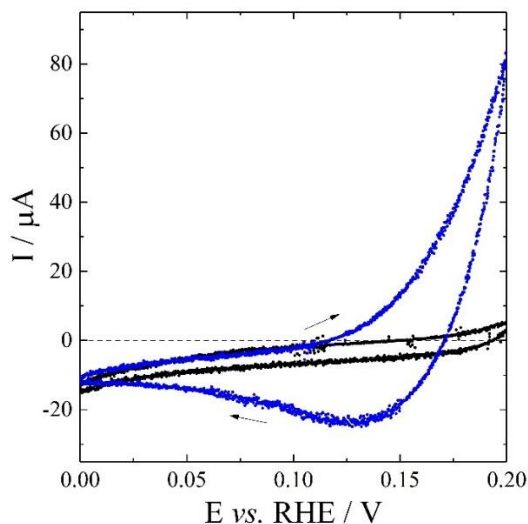


Figure 16: Cyclic voltammetry of the Cu|H₂SO₄ (black line) and Cu|H₂SO₄,phen (blue line) systems at $dE/dt = 0.02 \text{ V s}^{-1}$ in the potential window of 0 to 0.20 V. $[\text{H}_2\text{SO}_4] = 0.5 \text{ mol L}^{-1}$ and $[\text{phen}] = 1.5 \text{ mmol L}^{-1}$.

As observed, these values do not show big discrepancies between each other and are approximately 10 times lower than those expected to the adsorption of one phen molecule (with molar mass equal to 180.2 g mol^{-1}) in a one-electron process, which is $1868 \text{ } \mu\text{g C}^{-1}$, as follows:

$$m/z = \frac{180.2 \text{ g mol}^{-1}}{1 \times 96485 \text{ C mol}^{-1}} = 1868 \text{ } \mu\text{g C}^{-1} \quad \text{Eq. 17}$$

This suggests that an unknown charge transfer processes occurs simultaneously at this potential window. In certain extension, the adsorption of protonated phen can be considered a fast equilibrium with the dissolved molecules in the interface, which modifies the total coverage of the adsorbed species and ends up with underestimated values of m/z . In the next sections we will provide a more realistic information, or physical sense, by converting m/z ratios in apparent molar mass and, finally, propose a kinetic mechanism to the emergence of the BS.

4.4. Scanning Electron Microscopy analysis

Corroborating with the previous measurements, this section will support the overall discussion by extracting surface images with the aid of the SEM. Nakanishi *et al.*⁶³ have

inspected the electrodeposit surface and observed two type of surface morphologies during the electrochemical oscillations: leaflet-like particles of a few micrometers in size and dense round-shaped leaflets, which are associated with low and high current states, respectively. Cu leaflets would occur in an anisotropic crystal growth by a selective adsorption on a specific crystalline facet inhibiting the global reaction. Interestingly, in a bistable state, the addition of phen resulted in a completely different morphology, reflecting the emergence of structured surfaces driven by distinct dynamic instabilities.

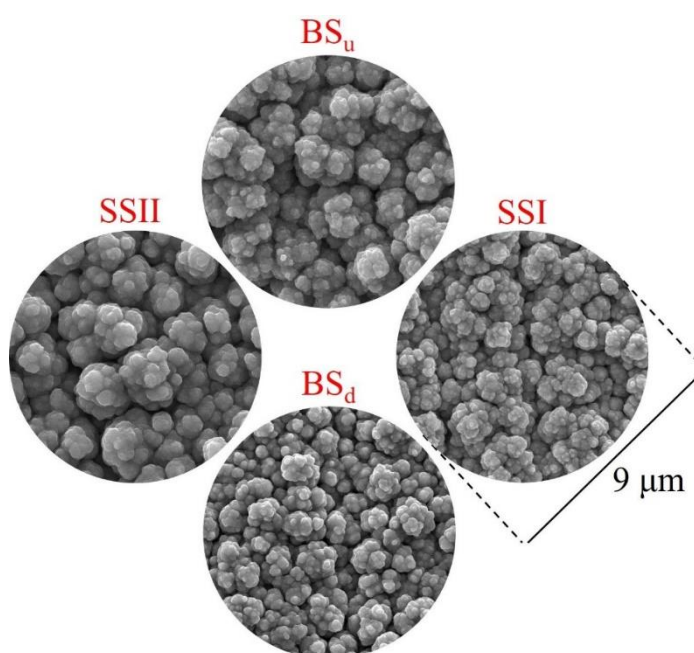


Figure 17: Electronic micrographs of the electrode surface after the electrodeposition of Cu perturbed with $2.0\ \text{mmol L}^{-1}$ of phen. The samples were obtained at the potentials of 0.24 (SSI), 0.12 (BS_u and BS_d as the upper and lower branches of the BS domain, respectively) and $-0.05\ \text{V}$ (SSII). The diameter of all images is $9\ \mu\text{m}$.

Figure 17 depicts SEM images of the surface at three applied voltages: $0.24\ \text{V}$ (SSI), $0.12\ \text{V}$ (bistability, upper (BS_u) and lower (BS_d) branches) and $-0.05\ \text{V}$ (SSII). The images show that the surface morphology of the electroplated deposit depends on the applied voltage. Regarding the SSI, the potential region where phen alters slightly the current density (**Figure 7**), a fine globular structure is clearly seen. As the potential slowly decreases, this fine structure moves towards a roundish nodule morphology, vide BS_d . Then, after the abrupt

suppression of the current by the adsorption of reaction intermediates the system reaches a state where massive deposition of Cu takes place.

The image took in the SSII represents this situation and evidences the production of thick Cu films which are coarse-grained and uniform along the electrode. Similar observations have been reported in the electrodeposition of copper.^{91,92} Finally, in the reverse scan, the surface structure gradually changes to a finer globular formation again as seen in BS_u. However, this return is not totally completed to SSI state and visual differences are observed in the images found at BS_u and BS_d. Overall, BS_u surface structure has a lower number of fine nodulations and embranchments compared to BS_d. According to the surface inhibition provoked by the addition of phen, these molecules seems to prevent the formation of coarse-grained structures since it demonstrates a substantial inhibiting effect in the reaction of Cu deposition.

Energy Dispersive X-ray Spectroscopy analysis were performed at the surface to detect what are the main elements at the surface studied. No significant signal that could be related to carbon and oxygen elements were detected during analysis in several points in the sample. Also, no signal related to the platinum substrate was observed. This indicates that the electrodeposited material is in fact a thick layer of metallic copper.

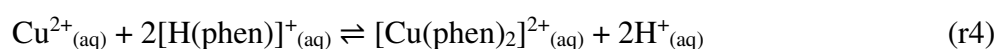
4.5. Mechanistic Interpretation

The initial voltammetric characterization presented in **Figure 7** attests the inhibition effect of the phen in the electrodeposition of Cu. In fact, it has been proposed by Nakanishi that metallic complexes have a strong adsorption on the copper surface, which reduce the total active area.⁶³ Phen molecules have also a favorable interaction with metallic surfaces⁹³⁻⁹⁶ and can easily change its orientation depending on the applied voltage.^{97,98} Therefore, not only the metallic complexes could induce dynamic instabilities but also the ligands by a significant adsorption process. Herein, we provide mechanistic information about the effect of the blocking species using a combination of surface techniques.

Firstly, it is important to consider that the reaction media, where the study was conducted, is highly acidic with $[\text{H}_2\text{SO}_4] = 0.5 \text{ mol L}^{-1}$ and $[\text{CuSO}_4] = 0.5 \text{ mol L}^{-1}$ or $\text{pH} \rightarrow 0$. As the pK_a of the $[\text{H}(\text{phen})]^+$ and $[\text{H}(\text{phen})_2]^+$ species are 5.12 and 2.11, respectively, as discussed before in section 1.3. Hence, for $\text{pK}_a > \text{pH}$ it is expected to observe the reactions of

phen protonation, (r1) and (r2) in the bulk of the solution. For the sake of simplicity, we neglected the contribution of the $[\text{H}(\text{phen})_2]_{(\text{aq})}^+$ species in the analysis (r2), although it has been also detected experimentally in a self-stacking mechanism.^{68,99}

Because copper sulfate is also presented in the electrochemical cell, we expect the complexation reaction to occur in a small extension, (r4), since the complexation of protonated phen species, $[\text{H}(\text{phen})]^+$ with Cu^{2+} is unfavorable due to issues of low acid-base affinity. The copper cation is a Lewis acid and its affinity with the phen molecule is decreased when the last one is protonated.

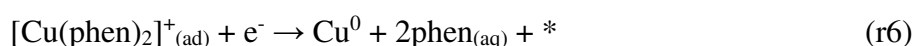


Nakanishi⁶³ proposed that the complex species, $[\text{Cu}(\text{phen})_2]^{2+}$, can adsorb on the substrate surface and compete in parallel with the deposition of Cu. The electrochemical reduction of Cu^{2+} in the solid/liquid interface takes place in a two-electron transfer, as discussed before in (r3). This reaction proceeds through two steps and the rate determinant step is considered to be the first electron reception by the bivalent ion.¹⁰⁰ We write this reaction in a short well-known form (r3). On the other hand, the electrons transfer in the metallic complex might happen in an adsorption pathway,⁶³

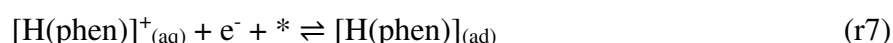


in our electrochemical mechanism asterisk means free active sites on the surface. The nature of the adsorbed complex is still not clear but experimental evidences in different substrates, concentrations and solution pH have shown to be $[\text{Cu}(\text{phen})_2]_{(\text{ad})}^+$.¹⁰¹⁻¹⁰³ Nevertheless, in very strong acidic media as ours, the protonation of the nitrogen in the phen molecules is energetically favorable. Because of the positively charged reactants, the formation of the coordinated bonds is not easily performed, and a complex dissociation would occur as well.

The complexed adsorbed species own a short lived-state and are rapidly reduced to metallic Cu in lower potentials,^{101,102} (r6). In this reaction the phen ligands dissociate and are released into the solution:



Larger concentrations of phen result in steeper slopes j vs E during the inhibition process and a shift to less negative potentials. As the dynamic equilibrium of the has an impact on the total coverage of the adsorbed metallic complexes, the mass variations would be associate mainly with the electrochemical deposition of Cu. The reduction evolving a metallic complex should shift the onset potential, but it is not verified in our experiments. Although the concentration of phen is much lower than $\text{Cu}^{2+}_{(\text{aq})}$, a fast equilibrium might be observed by those protonated molecules which are not coordinated with Cu, (r7):



The adsorption pathway through a reduction reaction is consistent with the results displayed in **Figure 15**: (a) j vs E , (b) Δm vs E , (c) Δm vs q in the potential interval of 0-0.20 V in the absence of CuSO_4 . The curves follow the color code used as previously: 0.5 (green), 1.0 (blue) and 2.0 mmol L^{-1} (red). $[\text{H}_2\text{SO}_4] = 0.5 \text{ mol L}^{-1}$. and **Figure 16**. Higher reduction and oxidation currents are detected for increasing phen concentrations, associated with the mass variations obtained from the EQCN measurements, in which the mass increase is associated with the negative current values due to the adsorption process and dissociation leads to the mass decrease.

We can now use the m/z ratios obtained in section 4.3 and convert them to apparent molar mass (M_{app}) considering the faradaic process. It is called apparent since some deviations from the expected molar mass values can occur, the timescale used in our experiments might not always be appropriate for the detection of some process, such as the fast or really slow ones. Obtaining underestimated or overestimated molar mass values might happen in these cases, the technique has a limiting response, in which too fast mass variations cannot be detected.

Figure 14 provides the following information in each concentration of phen: 352 $\mu\text{g C}^{-1}$ (0.5 mmol L^{-1}), 392 $\mu\text{g C}^{-1}$ (1.0 mmol L^{-1}), 416 $\mu\text{g C}^{-1}$ (2.0 mmol L^{-1}). We already know that the electroreduction of Cu^{2+} has a theoretical value of 329 $\mu\text{g C}^{-1}$, and hence, the experimentally measured m/z ratios represent mostly the reaction (r3), the reduction of Cu^{2+} ions through a two-electron step reaction. This observation agrees with the large difference between the concentrations of CuSO_4 and phen in the reaction media and the massive electrochemical deposition of Cu during the gravimetric measurements. In this respect, the faradaic reactions (r5)-(r7) participate only with 23 $\mu\text{g C}^{-1}$ (0.5 mmol L^{-1}), 63 $\mu\text{g C}^{-1}$ (1.0 mmol L^{-1}), 87 $\mu\text{g C}^{-1}$ (2.0 mmol L^{-1}) because of the discount of 329 $\mu\text{g C}^{-1}$ from the total value.

These m/z ratios are quite small, and if the conversion is made for a 1 electron transfer reaction, they can be associated with M_{app} : 2.2, 6.1, 8.4 g mol⁻¹, respectively. The results point out that none of the metallic complex intermediates, containing Cu (63.5 g mol⁻¹) or phen (180.2 g mol⁻¹), could be adsorbed on the surface due to their high molar mass, they all would have much larger molar mass than all the ones detected in our experiments. Note that our model does not take account the participation of water molecules and (bi)sulfate anions dissolved in the electrolyte and, possibly, those small changes could be also related to it.

On the basis of these experimental results, we can conclude that the adsorbed intermediates do not alter mass variations significantly during the formation of the NDR but can inhibit the reduction of copper ions and modify drastically the global faradaic reaction as observed in **Figure 7** and **Figure 13**. It was found that phen molecules are adsorbed vertically on Cu(111) with their nitrogen atoms facing the substrate.⁹⁸ The molecules were stacked to form polymer-like chains because of the π -electron attraction in the aromatic ring among them. The adlayer of phen formed on Cu surface changes depending on the applied voltage and it is considered more organized in positive potentials. If the electrolyte is kept in acidic conditions the molecular plane of phen is inclined toward the metal surface⁹³ which could further enhance the inhibition factor.

Our experimental results converge to the idea that the inhibiting effect of the global faradaic reaction could be related with the adsorption of phen – the protonated phen molecules coordinate with Cu²⁺ in a negligible extension due to the highly acidic media (two positively charged reactants). Then, reactions (r5) and (r6), which represent the reduction of copper ions by the complexation and adsorption pathway, should not be present, or at least present in a non-significant extent, and the equilibrium in the reaction of the complex formation (r4) should be definitely shifted to the left. Additionally, the adsorption of protonated phen on the Cu surface might occur in a fast equilibrium with the molecules on the interface, impacting on the total coverage of the adsorbed species and resulting in underestimated values of m/z , vide **Figure 14** and **Figure 15**. It might be also considered a weak adsorption driven possibly by physical interactions which does not contribute to meaningful mass variations, but still affects the faradaic reaction of the electrochemical reduction of Cu.

5. Conclusion

5.1. General conclusions

We have studied the effect of 1,10-phenanthroline (phen) in the electrochemical reduction of Cu under strong acidic media by means of different surface techniques. Overall, phen molecules are found to be protonated and the coordination with copper ions dissolved in the solution seems to be unfavorable. The phen molecules adsorb on the surface and inhibits the reduction of Cu^{2+} from the solution. This blocking process alters significantly the area of the electrode and induces an autocatalytic evolution of the double layer potential. As experimentally observed, this dynamic behavior promotes the formation of a bistable domain, delineated by a saddle-node bifurcation, in a wide range of controlling parameters, such as: the external resistance, the applied voltage and the concentration of phen.

The increase of the concentration of phen favors a shrinkage of the bifurcation diagram and shifts it to less negative potentials. Besides voltammetric characterization, the Electrochemical Impedance Spectroscopy measurements also converge to a conclusion of an inhibiting process. The instability generated by adsorption was confirmed by the hidden negative impedance, that is, $Z'(\omega) < 0$ for $\omega \neq 0$, indicating a HN-NDR system. The Electrochemical Quartz Crystal Nanobalance experiments show that the mass variations take place mainly by the electrodeposition of Cu from the bivalent ions, Cu^{2+} , and consequently, the adsorption of dissolved phen molecules does not show an important contribution in this respect.

A kinetic mechanism is proposed based on the observations, and a good agreement is obtained between the apparent molar mass extracted from experiments and the theoretical values. Surface images indicate that phen prevents the formation of coarse-grained structures and the BS domain is composed by two different surface morphologies – the lower branch has finer nodulations compared to the upper branch. Finally, we believe that our results can trigger the design of a switchable surface electrodes taking advantage from the easy access to a bistable behavior. A reversible change in the coverage of the phen could turn “on” or “off” two different surface states multiple times.

5.2. Perspectives

Currently a new project, concerning the detailed study of the effect of azobenzenes in the electrodepositing of copper is being developed by a student in our group. This work has a purpose of being an extension of this one. The experimental features are quite similar, as they will be placed in acid media containing sulfate copper salt, in a similar three-cell array. An azobenzene is an organic compound, composed of two phenyl rings connected by a N=N double bond, the term azobenzene refers to the wide class of similar compounds with these attributes. These compounds are known for their isomerization in specific wavelengths, that is, a structural and reversible modification occurs between the states *cis* and *trans*, known as photosteady-states, when they are irradiated by UV-visible light. It is well-known that the affinity of organic compounds can be modified in different isomers, and these differences are detectable and can be identified in electrochemical experiments.¹⁰⁴

The project proposes the study and control of the formation of self-organized and nanostructured structures during non-linear phenomena in the reaction of electrodeposition of copper with the presence of azobenzene molecules. The control of the photoisomerization of the azobenzenes molecules with the irradiation of UV-visible light will be exploited to manipulate the thickness of metallic nanolayers in an oscillatory regime. The control will be carried out by irradiating light in the UV-visible region which, in turn, induces a change in the *cis* or *trans* molecular geometry depending on the wavelength of the radiation. Therefore, this type of photoswitch will allow precise control of the thickness of the deposit in the cathodic deposition regime.

6. Bibliography

- (1) Gewirth, A. A.; Andricacos, P. C.; Switzer, J. A.; Dukovic, J. O. Hot Topics in Electrodeposition. *Electrochemical Society Interface* **1998**, 7 (1), 22–27.
- (2) Nakanishi, S. Self-Organized Formation of Layered Nanostructures by Oscillatory Electrodeposition. In *Nanostructured Materials in Electrochemistry*; 2008; pp 267–290.
- (3) Hamann, C. H.; Hamnett, A.; Vielstich, W. *Electrochemistry*; 2nd edition, Wiley-VCH, 2007.
- (4) Ihara, D.; Nagai, T.; Yamada, R.; Nakanishi, S. Interfacial Energy Gradient at a Front of an Electrochemical Wave Appearing in CuSn-Alloy Oscillatory Electrodeposition. *Electrochimica Acta* **2009**, 55 (2), 358–362.
- (5) Eskhult, J.; Herranen, M.; Nyholm, L. On the Origin of the Spontaneous Potential Oscillations Observed during Galvanostatic Deposition of Layers of Cu and Cu₂O in Alkaline Citrate Solutions. *Journal of Electroanalytical Chemistry* **2006**, 594 (1), 35–49.
- (6) Leopold, S.; Herranen, M.; Carlsson, J.-O. Spontaneous Potential Oscillations in the Cu(II)/Tartrate and Lactate Systems, Aspects of Mechanisms and Film Deposition. *Journal of The Electrochemical Society* **2001**, 148 (8), C513-C517.
- (7) Bohannon, E. W.; Huang, L.-Y.; Miller, F. S.; Shumsky, M. G.; Switzer, J. A. In Situ Electrochemical Quartz Crystal Microbalance Study of Potential Oscillations during the Electrodeposition of Cu/Cu₂O Layered Nanostructures. *Langmuir* **1999**, 15 (3), 813–818.
- (8) Switzer, J. A.; Maune, B. M.; Raub, E. R.; Bohannon, E. W. Negative Differential Resistance in Electrochemically Self-Assembled Layered Nanostructures. *The Journal of Physical Chemistry B* **1999**, 103 (3), 395–398.
- (9) Krastev, I.; Dobrovolska, T. Pattern Formation During Electrodeposition of Alloys. *Journal of Solid State Electrochemistry* **2013**, 17 (2), 481–488.
- (10) Cheng, X.; Zhang, J.; Chang, H.; Luo, L.; Nie, F.; Feng, X. High Performance Cu/Cu₂O Nanohybrid Electrocatalyst for Nonenzymatic Glucose Detection. *Journal of Materials*

Chemistry B **2016**, 4 (27), 4652–4656.

- (11) Rehnlund, D.; Valvo, M.; Tai, C.-W.; Ångström, J.; Sahlberg, M.; Edström, K.; Nyholm, L. Electrochemical Fabrication and Characterization of Cu/Cu₂O Multi-Layered Micro and Nanorods in Li-Ion Batteries. *Nanoscale* **2015**, 7 (32), 13591–13604.
- (12) Orlik, M. *Self-Organization in Electrochemical Systems I*; Springer-Verlag, Ed.; Berlin, 2012.
- (13) Nicolis, G.; Prigogine, I. *Self-Organization in Nonequilibrium Systems: From Dissipative Structures to Order Through Fluctuations*; Wiley: New York, 1977.
- (14) Scott, S. K. *Oscillations, Waves, and Chaos in Chemical Kinetics*; Oxford University Press: Oxford, 1994.
- (15) Epstein, I. R.; Pojman, J. A. Introduction to Nonlinear Chemical Dynamics. Oscillations, Waves, Patterns and Chaos. Oxford University Press: New York, **1998**.
- (16) Field, R. J.; Koros, E.; Noyes, R. M. Oscillations in Chemical Systems. II. Thorough Analysis of Temporal Oscillation in the Bromate-Cerium-Malonic Acid System. *Journal of the American Chemical Society* **1972**, 94 (25), 8649–8664.
- (17) Golden, T. D.; Raffaele, R. P.; Switzer, J. A. Cross-Sectional Scanning Tunneling Microscopy of Electrodeposited Metal Oxide Superlattices. *Applied Physics Letters* **1993**, 63 (11), 1501–1503.
- (18) Leopold, S.; Herranen, M.; Carlsson, J.-O. Spontaneous Potential Oscillations in the Cu(II)/Tartrate and Lactate Systems, Aspects of Mechanisms and Film Deposition. *Journal of The Electrochemical Society* **2001**, 148 (8), C513–C517.
- (19) Switzer, J. A.; Hung, C.-J.; Huang, L.-Y.; Miller, F. S.; Zhou, Y.; Raub, E. R.; Shumsky, M. G.; Bohannon, E. W. Potential Oscillations During the Electrochemical Self-Assembly of Copper/Cuprous Oxide Layered Nanostructures. *Journal of Materials Research* **1998**, 13 (04), 909–916.
- (20) Silverberg, J. L.; Na, J.; Evans, A. A.; Liu, B.; Hull, T. C.; Santangelo, C. D.; Lang, R. J.; Hayward, R. C.; Cohen, I. Origami Structures with a Critical Transition to Bistability Arising from Hidden Degrees of Freedom. *Nature Materials* **2015**, 14, 389–393.

- (21) Sato, O. Dynamic Molecular Crystals with Switchable Physical Properties. *Nature Chemistry* **2016**, *8*, 644–656.
- (22) Hagiwara, H.; Masuda, T.; Ohno, T.; Suzuki, M.; Udagawa, T.; Murai, K. Neutral Molecular Iron(II) Complexes Showing Tunable Bistability at Above, Below, and Just Room Temperature by a Crystal Engineering Approach: Ligand Mobility into a Three-Dimensional Flexible Supramolecular Network. *Crystal Growth Design* **2017**, *17*, 6006–6019.
- (23) Wu, D.; Shao, D.; Wei, X.; Shen, F.; Shi, L.; Kempe, D.; Zhang, Y.; Dunbar, K. R.; Wang, X.; Wu, D.; Reversible On-Off Switching of a Single-Molecule Magnet via a Crystal-to-Crystal Chemical Transformation. *Journal of the American Chemical Society* **2017**, *139*, 11714–11717.
- (24) Amirjalayer, S.; Martinez-Cuezva, A.; Berna, J.; Woutersen, S.; Buma, W. J. Photoinduced Pedalo-Type Motion in an Azodicarboxamide-Based Molecular Switch. *Angewandte Chemie International Edition* **2018**, *57* (7), 1792–1796.
- (25) Mukoyama, Y.; Kawasaki, H.; Hara, D.; Yamada, Y. Appearance of New Oscillations (Named Oscillations I and J) during Reduction of H₂O₂ on Platinum Electrode. *Journal of Electrochemical Society* **2017**, *164* (9), H675–H684.
- (26) Mukoyama, Y.; Kawasaki, H.; Hara, D.; Yamada, Y.; Nakanishi, S. Appearance of New Oscillation (Named Oscillation H) Induced by Na₂SO₄ and K₂SO₄ in Electroreduction of H₂O₂ on Platinum. *Journal of The Electrochemical Society* **2017**, *164* (2), H1–H10.
- (27) Krischer, K.; Varela, H. Oscillations and Other Dynamic Instabilities. In *Handbook of Fuel Cells: Fundamentals, Technology and Applications*; 2010; pp 679–701.
- (28) Krischer, K.; Haber, F.; Nonlinear Dynamics in Electrochemical Systems. In *Advances in Electrochemical Science and Engineering*; Wiley-VCH Verlag GmbH & Co., 2002; Vol. 8, pp 89–208.
- (29) Krischer, K. Principles of Temporal and Spatial Pattern Formation in Electrochemical Systems. In *Modern Aspects of Electrochemistry*; Conway, B. E., Bockris, J. O., White, R. E., Eds.; Kluwer Academic Publishers: Boston, 1999; Vol. 32, pp 1–142.

- (30) Koper, M. T. M. The Theory of Electrochemical Instabilities. *Electrochimica Acta* **1992**, 37 (10), 1771–1778.
- (31) Dörfler, H.-D.; Müller, E. The Analysis of Current Oscillations on the Basis of the Retardation of Electrode Processes by Different Surfactants. *Journal of Electroanalytical Chemistry and Interfacial Electrochemistry* **1982**, 135 (1), 37–53.
- (32) Bockris, J. O.; Reddy, A. K. N. *Volume 2 Modern Electrochemistry*; Springer US: Boston, MA, 1973.
- (33) *Advances in Electrochemical Science and Engineering*; Alkire, R. C., Kolb, D. M., Eds.; Wiley-VCH Verlag GmbH & Co. KGaA: Weinheim, FRG, 2002; Vol. 8.
- (34) Wilhelm, T. The Smallest Chemical Reaction System with Bistability. *BMC Systems Biology* **2009**, 3 (90), 1–9.
- (35) Kouvaris, N. E.; Kori, H.; Mikhailov, A. S. Traveling and Pinned Fronts in Bistable Reaction-Diffusion Systems on Networks. *PLoS ONE* **2012**, 7 (9), e45029.
- (36) Crespo-Yapur, D. A.; Bonnefont, A.; Schuster, R.; Krischer, K.; Savinova, E. R. Sequential Activation and Oscillations of Globally Coupled Microelectrodes during a Bistable Reaction. *ChemElectroChem* **2014**, 1 (6), 1046–1056.
- (37) Kouvaris, N. E.; Sebek, M.; Mikhailov, A. S.; Kiss, I. Z. Self-Organized Stationary Patterns in Networks of Bistable Chemical Reactions. *Angewandte Chemie International Edition* **2016**, 55 (42), 13267–13270.
- (38) Bozdech, S.; Biecher, Y.; Savinova, E. R.; Schuster, R.; Krischer, K.; Bonnefont, A. Oscillations in an Array of Bistable Microelectrodes Coupled through a Globally Conserved Quantity. *Chaos* **2018**, 045113 (28), 1–10.
- (39) Gogia, G.; Burton, J. C. Emergent Bistability and Switching in a Nonequilibrium Crystal. *Physical Review Letters* **2017**, 178004 (119), 1–5.
- (40) De Kepper, P.; Boissonade, J. Theoretical and Experimental Analysis of Phase Diagrams and Related Dynamical Properties in the Belousov-Zhabotinskii System. *The Journal of Chemical Physics* **1981**, 75 (1), 189–195.

- (41) Boissonade, J.; De Kepper, P. Transitions from Bistability to Limit Cycle Oscillations. Theoretical Analysis and Experimental Evidence in an Open Chemical System. *Journal of Physical Chemistry* **1980**, *84*, 501–506.
- (42) Ouyang, Q. ; Nosticzius, Z. ; Swinney, H. L. Spatial Bistability of Two-Dimensional Turing Patterns in a Reaction-Diffusion System. *Journal of Physical Chemistry* **1992**, *96*, 6773–6776.
- (43) Kaminaga, A.; Vanag, V. K.; Epstein, I. R. A Reaction–Diffusion Memory Device. *Angewandte Chemie International Edition* **2006**, *45* (19), 3087–3089.
- (44) Szalai, I.; De Kepper, P. Turing Patterns, Spatial Bistability, and Front Instabilities in a Reaction–Diffusion System. *The Journal of Physical Chemistry A* **2004**, *108* (25), 5315–5321.
- (45) Bar, M. ; Nettesheim, S. ; Rotermund, H. H. ; Eiswirth, M. ; Ertl, G. Transition Between Fronts and Spiral Waves in Bistable Surface Reaction. *Physical Review Letters* **1995**, *74* (7), 1246–1249.
- (46) Bodega, P. S.; Alonso, S.; Rotermund, H. H. Effects of External Global Noise on the Catalytic CO Oxidation on Pt(110). *Journal of Chemical Physics* **2009**, *130* (8), 1–7.
- (47) De Decker, Y.; Baras, F. Bistability and Explosive Transients in Surface Reactions: The Role of Fluctuations and Spatial Correlations. *European Physical Journal B* **2010**, *78* (2), 173–186.
- (48) Strogatz, S. H. *Nonlinear Dynamics and Chaos: With Applications to Physics, Biology, Chemistry, and Engineering*. Addison-Wesley: Cambridge, 1994.
- (49) *Advances in Chemical Physics*; Prigogine, I., Rice, S. A., Eds.; John Wiley & Sons, Inc.: Hoboken, NJ, USA, 1996; Vol. 14.
- (50) Jurczakowski, R.; Orlik, M. Bistable/Oscillatory System Based on the Electroreduction of Thiocyanate Complexes of Nickel(II) at a Streaming Mercury Electrode. Experiment and Simulation. *Journal of Physical Chemistry B* **2002**, *106* (5), 1058–1065.
- (51) Orlik, M.; Jurczakowski, R. On the Stability of Nonequilibrium Steady-States for the Electrode Processes at a Streaming Mercury Electrode. *Journal of Physical Chemistry B*

- 2002**, *106* (30), 7527–7536.
- (52) Jurczakowski, R.; Orlik, M. Experimental and Theoretical Studies of the Multistability in the Electroreduction of the Nickel(II)- N_3^- Complexes at a Streaming Mercury Electrode. *Journal of Physical Chemistry B* **2003**, *107*, 10148–10158.
- (53) Jurczakowski, R.; Orlik, M. Experimental and Theoretical Impedance Studies of Oscillations and Bistability in the Ni(II)- SCN^- Electroreduction at the Streaming Mercury Electrode. *Journal of Electroanalytical Chemistry* **2007**, *605* (1), 41–52.
- (54) Gorzkowski, M. T.; Jurczakowski, R.; Orlik, M. Electrochemical Oscillations and Bistability in the Redox Processes of Mercury Ions, Coupled with the Self-Induced Convection of Hg Surface. *Journal of Electroanalytical Chemistry* **2008**, *615* (2), 135–144.
- (55) Gorzkowski, M. T.; Orlik, M. Electrochemical Oscillations and Bistability during Anodic Dissolution of Vanadium Electrode in Acidic Media—Part II. The Model. *Journal of Solid State Electrochemistry* **2011**, *15* (11–12), 2321–2330.
- (56) Gorzkowski, M. T.; Wesołowska, A.; Jurczakowski, R.; Ślepski, P.; Darowicki, K.; Orlik, M. Electrochemical Oscillations and Bistability during Anodic Dissolution of Vanadium Electrode in Acidic Media—Part I. Experiment. *Journal of Solid State Electrochemistry* **2011**, *15* (11–12), 2311–2320.
- (57) Xuf, Y.; Schell, M. Bistability and Oscillations in the Electrocatalyzed Oxidation of Formaldehyde. *Journal of Physical Chemistry* **1990**, *94* (18), 7137–7143.
- (58) Cai, Xiarong ; Schell, M. Observation of Bistability in Cyclic Voltammetric Experiments on Ethanol, Propanol, Butanol and Formic Acid/Formate. *Electrochimica Acta* **2000**, *37* (4), 673–680.
- (59) Chen, S.; Schell, M. Bistability and Excitability in the Electrochemical Oxidation of Ethanol. *Electrochimica Acta* **1999**, *44* (26), 4773–4780.
- (60) Schell, M. Mechanistic and Fuel-Cell Implications of a Tristable Response in the Electrochemical Oxidation of Methanol. *Journal of Electroanalytical Chemistry* **1998**, *457*, 221–228.

- (61) Chen, S.; Schell, M. A Comparison of Multistability in the Electrocatalyzed Oxidations of Methanol and Ethanol in Acid and Alkaline Solutions. *Journal of Electroanalytical Chemistry* **1999**, *478*, 108–117.
- (62) Chen, S.; Schell, M. Excitability and Multistability in the Electrochemical Oxidation of Primary Alcohols. *Electrochimica Acta* **2000**, *45*, 3069–3080.
- (63) Nakanishi, S.; Sakai, S.; Nishimura, K.; Nakato, Y. Layer-by-Layer Electrodeposition of Copper in the Presence of o-Phenanthroline, Caused by a New Type of Hidden NDR Oscillation with the Effective Electrode Surface Area as the Key Variable. *The Journal of Physical Chemistry B* **2005**, *109* (40), 18846–18851.
- (64) Schlitter, F. W. ; Eichkorn, G. ; Fischer, H. Rhythmisch Lamerlles Kristallwachstum Bei Der Elektrolytischen Kupferabscheidung. *Electrochimica Acta* **1968**, *13*, 2063–2075.
- (65) Luman, C. R.; Castellano, F. N. Comprehensive Coordination Chemistry II. In *Transition*; Elsevier, 2003; Vol. 1, pp 25–39.
- (66) Swavey, S.; Brewer, K. J. Polyatomic Bridging Ligands. In *Comprehensive Coordination Chemistry II*; Elsevier, 2003; pp 135–157.
- (67) Bretti, C.; Crea, F.; Foti, C.; Sammartano, S. Solubility and Activity Coefficients of Acidic and Basic Nonelectrolytes in Aqueous Salt Solutions. 2. Solubility and Activity Coefficients of Suberic, Azelaic, and Sebacic Acids in $\text{NaCl}_{(\text{aq})}$, $(\text{CH}_3)_4\text{NCl}_{(\text{aq})}$, and $(\text{C}_2\text{H}_5)_4\text{NI}_{(\text{aq})}$ at Different Ionic Strengths at $t = 25^\circ \text{C}$. *Journal of Chemical & Engineering Data* **2006**, *51* (5), 1660–1667.
- (68) Mitchell, P. R. Hydrogen-1 Nuclear Magnetic Resonance Study of the Self-Association of 1,10-Phenanthroline, 2,2'-Bipyridyl, and Their Zinc(II) Complexes. *Journal of Chemical Society, Dalton Transactions* **1980**, *0* (7), 1079–1086.
- (69) Bencini, A.; Lippolis, V. 1,10-Phenanthroline: A Versatile Building Block for the Construction of Ligands for Various Purposes. *Coordination Chemistry Reviews* **2010**, *254* (17–18), 2096–2180.
- (70) Sugimasa, M.; Inukai, J.; Itaya, K. Adlayer of 1,10-Phenanthroline on Cu(111) in Acidic

- Solution. *Journal of The Electrochemical Society* **2003**, *150* (5), E266–E270.
- (71) Plieth, W. Additives in the Electrocrystallization Process. *Electrochimica Acta* **1992**, *37* (12), 2115–2121.
- (72) Armaroli, N. Photoactive Mono- and Polynuclear Cu(I)–Phenanthrolines. A Viable Alternative to Ru(II)–Polypyridines? *Chemical Society Reviews* **2001**, *30* (2), 113–124.
- (73) Calvo, E. J.; Etchenique, R. A. *Kinetic Applications of the Electrochemical Quartz Crystal Microbalance (EQCM)*; Elsevier Masson SAS, 2008; Vol. 37.
- (74) Gabrielli, C. Calibration of the Electrochemical Quartz Crystal Microbalance. *Journal of The Electrochemical Society* **1991**, *138* (9), 2657–2660.
- (75) Trasatti, S.; Petrii, O. A. Real Surface Area Measurements in Electrochemistry. *Pure* **1991**, *63* (5), 711–734.
- (76) Łukaszewski, M. Electrochemical Methods of Real Surface Area Determination of Noble Metal Electrodes – an Overview. *International Journal of Electrochemical Science* **2016**, *11*, 4442–4469.
- (77) Bockris, J. O. M.; Conway, B. E. Determination of the Faradaic Impedance at Solid Electrodes and the Electrodeposition of Copper. *The Journal of Physical Chemistry* **1985**, *28* (4), 707–716.
- (78) Grujicic, D.; Pesic, B. Electrodeposition of Copper: The Nucleation Mechanisms. *Electrochimica Acta* **2002**, *47*, 2901–2912.
- (79) Grujicic, D.; Pesic, B. Reaction and Nucleation Mechanisms of Copper Electrodeposition from Ammoniacal Solutions on Vitreous Carbon. *Electrochimica Acta* **2005**, *50*, 4426–4443.
- (80) Radisic, A.; Ross, F. M.; Searson, P. C. In Situ Study of the Growth Kinetics of Individual Island Electrodeposition of Copper. *Journal of Physical Chemistry B* **2006**, *110* (15), 7862–7868.
- (81) Abbott, A. P.; El Ttaib, K.; Frisch, G.; McKenzie, K. J.; Ryder, K. S. Electrodeposition

- of Copper Composites from Deep Eutectic Solvents Based on Choline Chloride. *Physical Chemistry Chemical Physics* **2009**, *11* (21), 4269–4277.
- (82) Nascimento, M. A.; Nagao, R.; Eiswirth, M.; Varela, H.; Coupled Slow and Fast Surface Dynamics in an Electrocatalytic Oscillator: Model and Simulations. *The Journal of Chemical Physics* **2014**, *141* (234701).
- (83) Strasser, P.; Eiswirth, M.; Koper, M. T. M. Mechanistic Classification of Electrochemical Oscillators - an Operational Experimental Strategy. *Journal of Electroanalytical Chemistry* **1999**, *478*, 50–66.
- (84) Burke, L. D.; Sharna, R. AC Impedance Investigation of Copper in Acid Solution I. Role of the High Energy Surface State. *Journal of Electrochemical Society* **2008**, *155* (1), D83–D90.
- (85) Shao, W.; Pattanaik, G.; Zangari, G. Electrochemical Nucleation and Growth of Copper from Acidic Sulfate Electrolytes on n-Si(001). *Journal of The Electrochemical Society* **2007**, *154* (7), D339–D345.
- (86) Chassaing, E.; Wiart, R. Epitaxial Growth and Electrode Impedance of Copper Electrodeposits. *Electrochimica Acta* **1984**, *29* (5), 649–660.
- (87) Wiart, R. Elementary Steps of Electrodeposition Analysed by Means of Impedance Spectroscopy. *Electrochimica Acta* **1990**, *35* (10), 1587–1593.
- (88) Gabrielli, C.; Moçotéguy, P.; Perrot, H.; Wiart, R. Mechanism of Copper Deposition in a Sulphate Bath Containing Chlorides. *Journal of Electroanalytical Chemistry* **2004**, *572* (2), 367–375.
- (89) Lee, C.; Anson, F. C. Electron Exchange between $\text{Cu}(\text{Phen})_2^+$ Adsorbed on Graphite and $\text{Cu}(\text{Phen})_2^{2+}$ in Solution. *Inorganic Chemistry* **1984**, *23* (7), 837–844.
- (90) Doe, H.; Yoshioka, K.; Kitagawa, T. Voltammetric Study of Protonated 1,10-Phenanthroline Cation Transfer across the Water/Nitrobenzene Interface. *Journal of Electroanalytical Chemistry* **1992**, *324*, 69–78.
- (91) Nichols, R. J.; Beckmann, W.; Meyer, H.; Batina, N.; Kolb, D. M. An in Situ Scanning Tunnelling Microscopy Study of Bulk Copper Deposition and the Influence of an

- Organic Additive. *Journal of Electroanalytical Chemistry* **1992**, 330 (1–2), 381–394.
- (92) Schmidt, W. U.; Alkire, R. C.; Gewirth, A. A. Mechanic Study of Copper Deposition onto Gold Surfaces by Scaling and Spectral Analysis of In Situ Atomic Force Microscopic Images. *Journal of Electrochemical Society* **1996**, 143 (10), 3122–3132.
- (93) Zawada, K.; Bukowska, J. An Interaction of 1,10-Phenanthroline with the Copper Electrode in Neutral and Acidic Aqueous Solutions: A Surface Enhanced Raman Scattering Study. *Journal of Molecular Structure* **2000**, 555, 425–432.
- (94) Muniz-Miranda, M.; Pergolese, B.; Bigotto, A. SERS and DFT Investigation on the Adsorption of 1,10-Phenanthroline on Transition Metal Surfaces. *Physical Chemistry Chemical Physics* **2010**, 12 (5), 1145–1151.
- (95) Andrade, G. F. S.; Temperini, M. L. A. 1,10-Phenanthroline Adsorption on Iron Electrode Monitored by Surface-Enhanced Raman Scattering (SERS). Comparison to SERS of Phen and Its Transition Metal Complex on Silver Electrode. *Journal of Physical Chemistry C* **2007**, 111 (37), 13821–13830.
- (96) Peng, Y.; Niu, Z.; Huang, W.; Chen, S.; Li, Z. Surface-Enhanced Raman Scattering Studies of 1,10-Phenanthroline Adsorption and Its Surface Complexes on a Gold Electrode. *Journal of Physical Chemistry B* **2005**, 109, 10880–10885.
- (97) Cunha, F.; Jin, Q.; Tao, N. J.; Li, C. Z. Structural Phase Transition in Self-Assembled 1,10'-Phenanthroline Monolayer on Au(111). *Surface Science* **1997**, 389, 19–28.
- (98) Sugimasa, M.; Inukai, J.; Itaya, K. Structure of Sulfur Adlayer on Cu(111) Electrode in Alkaline Solution. *Journal of The Electrochemical Society* **2003**, 150 (2), E110–E116.
- (99) Ishiguro, S.; Wada, H.; Ohtaki, H. Solvation and Protonation of 1,10-Phenanthroline in Aqueous Dioxane Solutions. *Bulletin of the Chemical Society of Japan* **1985**, 58 (3), 932–937.
- (100) Mattsson, E.; Bockris, J. O. Galvanostatic Studies of the Kinetics of Deposition and Dissolution in the Copper + Copper Sulphate System. *Transactions of the Faraday Society* **1959**, 55, 1586.
- (101) Čuljak, I.; Mlakar, M.; Branica, M. Cathodic Stripping Voltammetry of the Copper–

- 1,10-phenanthroline Complex. *Electroanalysis* **1995**, 7 (1), 64–69.
- (102) Quentel, F.; Madec, C. Voltammetric Study of the Copper-1,10-Phenanthroline Complex. *Analytica Chimica Acta* **1990**, 230, 83–90.
- (103) Sugiyama, K.; Aoki, K. Catalytic Reactions of Bis(1,10-Phenanthroline) Cuprous Complex with Hydrogen Peroxide at Glassy Carbon and Pyrolytic Graphite Electrodes. *Journal of Electroanalytical Chemistry* **1989**, 262, 211–219.
- (104) Asanuma, H.; Ito, T.; Yoshida, T.; Liang, X.; Komiyama, M. Photoregulation of the Formation and Dissociation of a DNA Duplex by Using the Cis-Trans Isomerization of Azobenzene. *Angewandte Chemie - International Edition* **1999**, 38 (16), 2393–2395.

7. Supplementary information

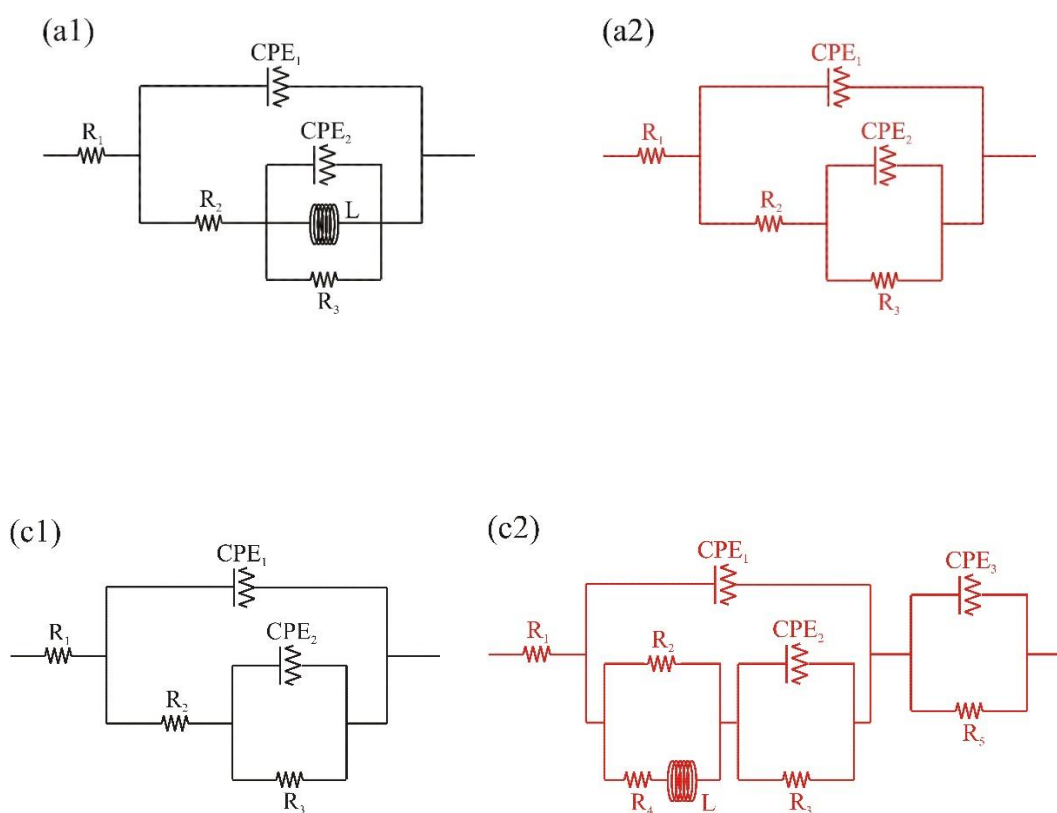


Figure S1. Equivalent circuits for the electrochemical impedance spectroscopy measurements showed in Figure 4 in the main text for plates a ($E = 0.24$ V) and c ($E = -0.05$ V), respectively. Index-1 represents the system $Pt|H_2SO_4, CuSO_4$ and index-2, same as index-1, but with the addition of 2.0 mmol L^{-1} of 1,10-phenantroline.

Table SI. Electrical parameters extracted by mathematical modeling of the impedance analysis using equivalent circuits represented in Figure S1.

Equivalent Circuits	a1	a2	c1	c2
$R_1 / \Omega \text{ cm}^2$	2.48	2.26	2.32	1.93
$R_2 / \Omega \text{ cm}^2$	9.94	10.3	1.62	3.12
$R_3 / \Omega \text{ cm}^2$	2.14	8.40	9.28	12.7
$R_4 / \Omega \text{ cm}^2$	-	-	-	252
$R_5 / \Omega \text{ cm}^2$	-	-	-	2.62
$\text{CPE}_1 / \Omega^{-1} \text{ cm}^{-2} \text{ s}^{n_1}$	116 μ	208 μ	335 μ	3.32 m
n_1	0.80	0.76	0.87	0.68
$\text{CPE}_1 / \text{F cm}^{-2}$	21.4 μ	29.9 μ	109 μ	-
$\text{CPE}_2 / \Omega^{-1} \text{ cm}^{-2} \text{ s}^{n_2}$	3.57 m	677 m	283 m	687 m
n_2	0.79	1.00	0.75	1.00
$\text{CPE}_2 / \text{F cm}^{-2}$	-	677 m	390 m	687 m
$\text{CPE}_3 / \Omega^{-1} \text{ cm}^{-2} \text{ s}^{n_3}$	-	-	-	38.8 m
n_3	-	-	-	0.96
$\text{CPE}_3 / \text{F cm}^{-2}$	-	-	-	35.3 m
$L / \text{H cm}^2$	63.3	-	-	18.6
χ^2	0.024	0.016	0.034	0.042